

# Accepted Manuscript

The North Atlantic inflow to the Arctic Ocean: High-resolution model study

Yevgeny Aksenov, Sheldon Bacon, Andrew C. Coward, A.J. George  
Nurser

PII: S0924-7963(09)00211-5  
DOI: doi: [10.1016/j.jmarsys.2009.05.003](https://doi.org/10.1016/j.jmarsys.2009.05.003)  
Reference: MARSYS 1863

To appear in: *Journal of Marine Systems*

Received date: 30 July 2008  
Revised date: 27 March 2009  
Accepted date: 27 May 2009



Please cite this article as: Aksenov, Yevgeny, Bacon, Sheldon, Coward, Andrew C., Nurser, A.J. George, The North Atlantic inflow to the Arctic Ocean: High-resolution model study, *Journal of Marine Systems* (2009), doi: [10.1016/j.jmarsys.2009.05.003](https://doi.org/10.1016/j.jmarsys.2009.05.003)

This is a PDF file of an unedited manuscript that has been accepted for publication. As a service to our customers we are providing this early version of the manuscript. The manuscript will undergo copyediting, typesetting, and review of the resulting proof before it is published in its final form. Please note that during the production process errors may be discovered which could affect the content, and all legal disclaimers that apply to the journal pertain.

**The North Atlantic Inflow to the Arctic Ocean: High-resolution Model Study**

YEVGENY AKSENOV\*, SHELDON BACON, ANDREW C. COWARD

AND A. J. GEORGE NURSER

National Oceanography Centre, Southampton

Waterfront Campus, European Way, Southampton, SO14 3ZH, UK

---

*Abstract*

North Atlantic Water (NAW) plays a central role in the ocean climate of the Nordic Seas and Arctic Ocean. Whereas the pathways of the NAW in the Nordic Seas are mostly known, those into the Arctic Ocean are yet to be fully understood. To elucidate these routes the results of a high-resolution global coupled ice-ocean model are used. We demonstrate that in 1989 - 2004 the NAW inflow was equally divided between the Fram Strait and Barents Sea. We find that salt influx within the branches is comparable but that most of the heat entered the Arctic Ocean through Fram Strait. The model shows complex NAW circulation patterns in the Barents Sea. Two mode waters in the Barents Sea branch are identified: a halocline water produced by surface cooling at shallow convective sites in the northern Barents Sea, and bottom water formed from NAW in the southeastern Barents Sea via full-depth convection and mixing. These two modes continue into the Nansen Basin along two separate routes: one through the northern Barents Sea shelf, and the other through the southeastern

---

\* Corresponding author. National Oceanography Centre, Southampton, University of Southampton, European Way, Southampton, SO14 3ZH, UK. Tel.: +44-(0)23-80599582; Fax: +44-(0)23-80596204. E-mail address: [yka@noc.soton.ac.uk](mailto:yka@noc.soton.ac.uk)

Barents Sea with halocline mode water dominating the outflow. Overall, less than half of the NAW coming into the Nordic Seas reaches the Arctic Ocean relatively unmodified, the rest of it will have been modified in the Barents and Kara Seas with a large fraction re-circulating into the North Atlantic.

*Keywords*

Arctic Ocean; Nordic Seas; North Atlantic Water; ocean modelling; oceanic transports; water mass transformation

**1. Introduction**

Oceanic exchanges between the North Atlantic Ocean and the Arctic Ocean, and particularly the inflow of North Atlantic Water (NAW) to the Eurasian Arctic, have been a focus of research over the last four decades. Much of the recent interest has been related to the large-scale shift to warmer climatic conditions in the Arctic Ocean that began in the early 1990s. Reported events providing evidence of this shift include: the long-term reduction of area and thinning of the Arctic sea ice cover (e.g. Lindsay and Zhang, 2005; Stroeve et al., 2005) including the record sea ice retreat in summer 2007 (e.g. Kay et al., 2008); the change in the sea ice drift pattern and upper ocean circulation (Polyakov and Johnson, 2000); the strengthening and warming of the Atlantic Inflow through Fram Strait (Schauer et al., 2004; Walczowski and Piechura, 2007, Holliday et al., 2008) and the intrusion of anomalously warm water into the central Arctic Ocean (e.g. Polyakov et al., 2005). These events are clear evidence of the recent change in the Arctic; whether or not it is caused by anthropogenic influences or natural variability is still uncertain. The Arctic Ocean itself influences the global climate. A range of global climate models have shown that the increased fresh water outflow from the Arctic due to increased precipitation,

continental runoff and glacial melt may slow down the Thermohaline Circulation in the North Atlantic (Stouffer et al., 2006; Vellinga and Wood, 2002; Wu et al., 2008).

To advance our knowledge of the oceanic climate in the Arctic and North Atlantic it is important to understand NAW circulation. NAW brings heat into ice-covered areas and forms the warm and salty layer in the Arctic Ocean (e.g. Steele and Boyd, 1998); it contributes to the formation of intermediate waters in the Arctic Ocean and plays a major part in the formation of the dense overflow waters across the Greenland-Scotland Ridge, ultimately affecting the North Atlantic deep western boundary current (Aagaard and Carmack, 1994; Rudels and Friedrich, 2000). The circulation of NAW in the Nordic Seas, Fram Strait and western Barents Sea has been extensively studied and is quite well understood, with few disputable features remaining (e.g. Blindheim and Østerhus, 2005). We know that the NAW flows across the Greenland-Scotland Ridge into the Iceland and Norwegian Seas and then north within the Norwegian Atlantic Current (e.g. Hansen and Østerhus, 2000) entering the Arctic Ocean through the Barents and Kara Seas as the Barents Sea Branch (BSB), and along the continental shelf break through the eastern Fram Strait as the Fram Strait Branch (FSB) (Schauer et al., 2002). However, in the Barents Sea despite the extensive temperature and salinity archives accumulated over the last century (Climatic Atlas of the Barents Sea: 1998; World Ocean Atlas 2005), only few year-long current-meter and synoptic Acoustic Doppler Currentmeter (ADCP) moorings are available in the northern and eastern areas of the sea, where the inflow of the NAW into the Arctic occurs (McClimans et al., 2000; Panteleev et al., 2007; Schauer et al., 2002); consequently the ocean circulation, interactions between the FSB and BSB and NAW modification in these areas are less well understood.

Modelling, verified with the help of long-term current meter measurements and sustained hydrographic observations in key locations, can help to overcome the paucity of observations, can provide an alternative to extensive *in-situ* observations to infer ocean circulation and can be useful in offering target hypotheses for observational campaigns on the quasi-synoptic scale. As the Rossby radius in the high-latitude Arctic is small, ocean models should have a high horizontal resolution to resolve eddies. High resolution also allows realistic ocean bottom topography to be used in the model, and this is essential to obtain realistic circulation in the Arctic. These models have been limited by computer power but multi-decadal global high-resolution simulations are now feasible. Sea ice models benefit from high resolution through the improved simulation of sea ice drift and redistribution.

The present study is aimed at the elucidation of the role of NAW in the Eurasian Arctic, and addresses the following questions: What were the pathways of NAW into the Arctic Ocean during the last two decades? What are the relative contributions of flows through Fram Strait and the Barents Sea to the NAW inflow into the Arctic? What are the mechanisms of the NAW modification in the Barents and Kara Seas? This paper is concerned only with the mean NAW inflow in the Arctic (annual cycle and inter-annual variability will be considered in later studies) and is structured as follows. Section 2 describes the model and experimental setup. Section 3 presents the NAW circulation from simulation results and summarises the observation-based knowledge; this section also evaluates the model's performance. Section 4 then uses the model results to describe the pathways and modification of NAW in the sparsely observed regions of the Barents and Kara Seas and its flow into the Arctic Ocean. Section 5 presents conclusions.

## 2. *Model and experimental set-up*

### 2.1 *Model*

The present study uses the results from a high-resolution global coupled ice-ocean general circulation model. The ocean model (OCCAM, Coward and de Cuevas, 2005) is a primitive equation-based Ocean General Circulation Model discretised on an Arakawa B-grid with  $1/12^\circ$  horizontal resolution. The ocean model covers the globe with two separate grids. The first for the Pacific, Indian Oceans, Southern Atlantic and Southern Ocean is a normal latitude-longitude geographical grid. The second grid for the North Atlantic and Arctic Ocean is a segment of the rotated spherical grid with poles placed on the geographical equator in the Pacific and Indian Oceans. The grids are joined along the Atlantic equator (where the grids are well-matched) and through the Bering Strait (via a linearised channel model), resulting in a nearly uniform global grid. The model has 66 levels in the vertical extending down to 6470 m and includes 27 levels in the upper 400 m with thickness ranging from 5.37 m in the uppermost layer to 48 m at 400 m and to 103 m at 1000 m. The *ca.* 5m resolution near the surface is fine enough for the KPP mixed-layer model to give a realistic evolution of the mixed-layer depth (Large et al., 1994), while the high resolution at intermediate depths allows the representation of the key vertical gradients, including those at the depth of halocline waters and in the NAW inflow. The model bathymetry was derived from the bathymetry of Sandwell and Smith (1995) patched north of  $72.0^\circ\text{N}$  with the International Bathymetric Chart of the Arctic Ocean (IBCAO) dataset (Jakobsson et al., 2000). Some manipulation of the model bathymetry was performed: one-model-cell wide straits were opened up to the width of two model cells, straits less than one cell wide were closed and a minimum depth of two model levels was imposed to

avoid conflict between the free surface model and partial bottom cells (Pacanowski and Gnanadesikan, 1998).

The fine model resolution and use of a partial bottom cell scheme permit a good representation of the complex bathymetry of the Arctic Ocean and Nordic Seas. This, in turn, helps improve the simulation of topographically controlled currents, such as the Norwegian Atlantic Current and West Spitsbergen Current (WSC). Furthermore, the correct representation of bathymetry in the areas of the Barents and Kara Seas and accurate sill depths and widths for the key straits such as Denmark Strait, Fram Strait, and the straits of the Canadian Archipelago are desirable for simulating the exchange between the Arctic Ocean and the North Atlantic. Despite the high horizontal resolution (*ca.* 8 km), the ocean model is only eddy-permitting in the Arctic Ocean. However, the Arctic Ocean Boundary Current along the Siberian shelf is resolved, since the strong density gradients in the area increase the Rossby radius to 50-100 km.

The model employs a free surface formulation (Killworth et al., 1991) and uses the Modified Split-QUICK advection scheme (Webb et al., 1998) to advect tracers and sea ice. On lateral boundaries the no-slip condition is applied. The sea ice model is configured on the same B-grid as the ocean and comprises sea ice dynamics with Elastic-Viscous-Plastic rheology (Hunke, 2001), and ice thermodynamics derived from the Semtner 3-layer model (Semtner, 1976). The sea ice thermodynamics also includes: lateral and bottom ice melting, partial freeze-up of open ocean, albedo dependency on snow/ice surface temperature. Excessive snow load results in sea ice flooding and snow-ice formation. Sea ice is embedded into the upper oceanic layer conserving volume in the sea ice-ocean system, thus making ice-ocean coupling more realistic (Aksenov, 2002). We did not use the dynamical embedding by Heil and

Hibler (2002), as it was not available for Ocean General Circulation models (OGCMs) at that time, and solve ocean and ice momentum balance equations separately. Our scheme is similar to the recently developed coupling scheme described by Campin et al. (2008). The dynamical coupling between sea ice and ocean is done via the quadratic drag law which uses the shear between the sea ice drift and ocean upper layer velocity, with turning angle set to zero (McPhee, 1984). The coupling is performed on each baroclinic time step of the ocean model allowing the full variability of the dynamical forcing to be applied to the ice-ocean system. The advantage of this approach is to subject the ice and ocean to high frequency wind forcing, which has been found extremely important not only for the correct development of the small scale ocean features, but also for the general ocean circulation (Leppäranta and Omstedt, 1990). The disadvantage of such approach is the necessity to integrate a sea ice model with the time step as short as the ocean model baroclinic time step.

To compensate for the absence of continental run-off and to prevent salinity drift, the simulated surface salinity is relaxed to the observed monthly climatological values (Boyer et al., 1998) on a time scale equivalent to 30 days for the top 20 m. No salinity relaxation is applied in the deep ocean (Webb et al., 1998). The relaxation is equivalent to adding  $104 \pm 16$  mSv of fresh water in the model for the Arctic Ocean alone and  $160 \pm 16$  mSv for the Arctic Ocean, the Barents Sea and the Nordic Seas. Those are in the range of corresponding estimates of continental runoff of 99-135 mSv and 122-165 mSv cited by Barry and Serreze (2000) and Dickson et al. (2007). Relaxation of the surface salinity to climatology also indirectly accounts for iceberg discharge, *ca.* 18 mSv, following Dickson et al. (2007), and terrestrial ice melt; there is no explicit description of these processes in the model.

The coupled sea ice-ocean model is forced with 6-hourly the US National Centers for Environmental Prediction (NCEP) 10-m height wind and sea level pressure, and with heat and moisture fluxes calculated from the 6-hourly 2-m height atmospheric temperature and specific humidity from NCEP re-analyses 1985-2004. The fluxes are calculated from bulk formulae for the atmospheric boundary layer and take into account the simulated sea surface temperature and boundary layer stability (Large et al., 1997). The model uses monthly precipitation (Spencer, 1993) blended with climatology for the later years; monthly cloudiness 1985-1991 (Rossow and Schiffer, 1991), updated with climatological data for the period 1992-2004; and monthly incoming solar radiation 1984-1991 (Bishop and Rossow, 1991), with gaps filled by climatology. Linear time interpolation is used to derive atmospheric field values that feed into the bulk formulae at each model timestep. Additionally, a diurnal cycle of solar radiation is implemented by distributing local daily mean solar radiation (calculated from linear time interpolation of the monthly fields) over the available hours of daylight at each location. The value used is scaled with a factor related to the sine of the solar elevation. The algorithm both simulates a local diurnal cycle and ensures that the net solar radiation over any 24 hour period is the same as that which would result from using simple linear time-interpolated values at each model timestep. A two-band approximation for the penetrative solar radiation (Paulson and Simpson, 1977) is used assuming a Jerlov Ib water type everywhere (Jerlov, 1968).

## **2.2 *Experimental set-up***

The coupled ice-ocean model ran for the period 1985-2004 with the ocean started from rest and from the initial ocean temperature and salinity fields derived from the merger of the Special Analysis Centre climatology (SAC) (Gouretski and Jancke,

1996), World Ocean Atlas data (Antonov et al., 1998; Boyer et al., 1998) and Arctic Ocean climatology (Steele et al., 2001). The initial sea ice and snow cover were taken from the Ice and Snow Atlas compiled by Romanov (1995). It was impossible for the model to reach a steady state during the 20-year-long run. However, because realistic initial ocean temperature, salinity and ice fields were used, most features of the global upper ocean circulation settled down during the first year of integration. Global mean kinetic energy (shown in Figure 1), heat and salt stayed fairly constant after the first three years of integration, whereas the barotropic component of the ocean circulation spun up within days. Sea ice volumes reached quasi-equilibrium within the first two years. We consider the model settled in a quasi-mean state after *ca.* 4 years and use the period 1989-2004 for analysis.

Model transports across key sections are not computed during the integrations, but are computed afterwards from the mean quantities. The monthly ocean velocity, sea surface height, temperature and salinity fields are obtained from sums of instantaneous fields updated every baroclinic time step. The use of monthly values instead of instantaneous fields does not affect volume transports but introduces low percentage errors in tracer transports due to coupling between ocean velocity and density, i.e. the mean of the product is not the same as the product of the means. The error bars on all model statistics are calculated as standard deviations from the multi-annual 1989-2004 average. Because the net volume transport across model sections is not zero the use of the term ‘heat transport’ is physically not exact. Instead we use term “quasi-heat transport” (e.g. Oliver and Heywood, 2003) throughout the paper and calculated it in a traditional way as a product of cross section velocity, area of section and temperature multiplied by heat capacity and water density (e.g. Gammelsrød et al., 2009). The calculations were referenced to the temperature of -

0.1°C to compare the model results with observations and previous model estimates; this temperature is the averaged temperature of the overall outflow from the Arctic Ocean (Aagaard and Greisman, 1975; Schauer et al., 2004). The “quasi-heat transport”, sometimes referred to as the ‘enthalpy transport’ (e.g. Schauer et al., 2004) has been a widely accepted diagnostics by the oceanographic and ocean modelling community as a proxy for the heat transport; the discussion of the *pro* and *contra* of this approach is beyond the scope of this paper. We calculated total salt transport referenced to the density of  $1027 \text{ kg m}^{-3}$ . To be consistent with the atmospheric forcing of the model we used pure water volumetric heat capacity of  $4.186 \cdot 10^6 \text{ J} \cdot \text{K}^{-1} \cdot \text{m}^{-3}$  (e.g. Simonsen and Haugan, 1996) instead of the lower values of  $4.088 \cdot 10^6 \text{ J} \cdot \text{K}^{-1} \cdot \text{m}^{-3}$  used for the upper ocean (e.g. Gill, 1982). This difference is not significant given the accuracy of the observational transports. The model sea ice and snow transports were obtained in the same manner with sea ice and snow densities of  $900 \text{ kg m}^{-3}$  and  $330 \text{ kg m}^{-3}$ . To diagnose convection in the model a ventilation tracer was used. Over the period from July 2000 to June 2002 the surface value of the ventilation tracer was relaxed towards unity with a rapid piston velocity of  $4.86 \cdot 10^{-4} \text{ m} \cdot \text{s}^{-1}$ . After June 2001, the surface flux relaxed the ventilation tracer back to zero. This relaxation flux was only applied over the ice-free part of the surface grid box.

### 3. *Simulated and observed NAW circulation*

In this section we present the simulated NAW inflow into the Arctic Ocean and compare the results to the available observations. We start from the Nordic Seas, Fram Strait and a region north of Svalbard, then go on to discuss the Barents Sea, Northern Barents Sea Shelf and Kara Sea. Model performance is judged on whether it simulates the realistic pattern and strength of the NAW inflow, whether this inflow is

at the right depth and has the correct temperature and salinity. All model velocities are mean-annual values unless otherwise stated. Figure 2 shows the bathymetry of the area and Figure 3 shows the simulated NAW circulation.

### 3.1 *NAW in the Nordic seas*

The model NAW inflow is compatible with observations (e.g. Hansen and Østerhus, 2000; Orvik and Niiler, 2002). The simulated NAW enters the Nordic Seas by crossing the Greenland-Scotland Ridge through the Faroe-Shetland Channel as the narrow, fast Shetland Current (SC, depth 0-610m, maximum speed  $0.22 \text{ m s}^{-1}$ ), between Iceland and the Faroe Islands as the meandering, fast Faroe Current (FC, depth 0-440m, maximum speed  $0.48 \text{ m s}^{-1}$ ), and through the eastern Denmark Strait as the ~55 km wide North Icelandic Irminger Current (NIIC, depth 0-315 m, maximum speed  $0.21 \text{ m s}^{-1}$ ). The SC forms the northward flow in the eastern Norwegian Atlantic Current (NwACE, Figure 3a) (Hansen and Østerhus, 2000; Orvik et al., 2001). The FC crosses the Iceland-Faroe Ridge through channels 420-490 m deep, proceeds eastwards following the Iceland-Faroes Front topographically locked to the ridge, then along the northern slope of the Faroe Plateau, contributing to the western Norwegian Atlantic Current (NwACW) (Hansen et al., 2003; Poulain et al., 1996) (Figure 3a). The simulated NIIC is the shallowest of the three branches (Østerhus et al., 2005); it flows east along the edge of the north Icelandic Shelf contributing to the NwACW. The model results and drifter trajectories offer evidence of the strong topographic steering of the NAW flow across the Greenland-Scotland Ridge (Jakobsen et al., 2003; Orvik and Niiler, 2002).

The model NwACE is a barotropic current steered by the bathymetry of the Norwegian Shelf break, consistent with current-meter data (Orvik et al., 2001). It

divides into the West Spitsbergen Current (WSC), which continues along the continental shelf break into Fram Strait, and the Nordkapp Current (NKC) which enters the Barents Sea. The separation occurs over a large part of the western Barents Sea Shelf 71°30'N-74°N as seen in drifter trajectories (Orvik and Niiler, 2002). The model baroclinic NwACW follows the Arctic Front between the Arctic waters and the NAW (Hansen and Østerhus, 2000; Orvik and Niiler, 2002). It flows towards Jan Mayen Island along the slopes of the Vøring Plateau, then northeastward along the Mohn Ridge forming the baroclinic western branch of the WSC found by Walczowski and Piechura (2007) (Figure 3a). This current follows the Mohn Ridge and Knipovich Ridge where it divides, with one part flowing westwards into the Greenland Sea along the periphery of the Greenland Sea Gyre and another part continuing along the Knipovich Ridge and converging with the proper WSC west of Svalbard.

In the Norwegian Sea the NAW layer is confined between the western and eastern cores of the North Atlantic Current; the zonal extent of the layer is *ca.* 600 km at 62-64°N and *ca.* 150 km at 76°N, which is in good agreement with observations (Mauritzen, 1996; Orvik and Skagseth, 2005; Furevik et al., 2007). The simulated temperature, salinity and maximum depth of the NAW core are also in agreement with the observations (Table 1). Both model and observations show deepening of the NAW layer towards the Norwegian Shelf (Orvik and Skagseth, 2005; Furevik et al., 2007) and in Lofoten Basin at 64°-69°N due to the deep counter-current (Orvik, 2004). Figure 4 depicts the salinity on the specific volume anomaly surface  $\Delta=2.1\text{e-}7\text{ m}^3\text{ kg}^{-1}$  from the observations (Rossby et al., 2007) and from the model. It shows that the pattern of the simulated NAW inflow, the position of the Arctic Front, and the location of the Greenland Sea Gyre are simulated accurately.

The simulated temperature and salinity of the NAW inflow across the Greenland-Scotland Ridge is close to the observed (Østerhus et al., 2005). However, compared to observations, the simulated inflow is slightly warmer and more saline in Denmark Strait, slightly colder and more saline over the Iceland-Faroe Ridge and colder in the Faroe-Shetland Channel (Table 2). Model temperature and salinity correspond to hydrographic sections in the Norwegian Sea (sections 1-7, Figure 3a) except for the Gimsøy section, where the NAW core is *ca.* 1.0°C colder than observed (Table 1). Both the model and observations show strong cooling (*ca.* 4.0°C) and slight freshening (0.16) of the NAW core on its way north (Tables 1 and 2).

The *ca.* 100 m deep and *ca.* 100 km wide Norwegian Coastal Current (NCC) originates from the Baltic Sea via the northern North Sea and bounds NwACE from the east, following the Norwegian coast along the 100 m contour into the Barents Sea. It carries low salinity Norwegian Coastal Water which provides sources of freshening for the NAW (Furevik, 2001; Loeng, 1991; Sætre, 1999).

### **3.2 NAW flow through Fram Strait and north of Svalbard**

Fram Strait is the deep channel (2500 m) connecting the Nordic Seas to the Arctic Ocean. The NAW flows through the strait along its eastern side as the upper 850 m part of the WSC (Fahrback et al., 2001; Schauer et al., 2004). The model simulates all known currents in Fram Strait (Schauer et al., 2004): the WSC and its branches, Yermak Plateau Branch (YPB) and Svalbard Branch (SVB), and the cold, fresh East Greenland Current flowing south on the western side of the strait (Figures 3b and 5). In addition, the model shows several westward re-circulations bifurcating from the WSC. The largest one, Knipovich Branch (KB), separates from the WSC, flows above the Knipovich Ridge and the Greenland-Spitsbergen sill, and joins the East Greenland

Current. Further north, at  $79^{\circ}$ - $79^{\circ}45'$ N, the remaining WSC splits into the SVB and the YPB (Figure 3b). The SVB, a narrow (40 km), upper shelf slope current, flows at 50-400 m with the mean velocity of  $0.14 \text{ m s}^{-1}$  (Figure 5), close to the observed one of  $0.10$ - $0.20 \text{ m s}^{-1}$  (Fahrbach et al., 2001). In Fram Strait, the YPB flows north as a surface-to-intermediate-depth current with a distinct velocity core located above the lower shelf slope (Figure 5). The simulated mean velocity in the YPB ( $0.09 \text{ m s}^{-1}$ ) agrees well with observations ( $0.04$ - $0.10 \text{ m s}^{-1}$  in Fahrbach et al., 2001).

In the northern part of the strait the model SVB turns east along the Spitsbergen coast making excursions into the trenches on the northern flanks of the Barents Sea shelf and interacting with the BSB, while the YPB follows the 1250-m contour of the western Spitsbergen Shelf and continues anticyclonically around the Yermak Plateau in agreement with observations (Saloranta and Haugan, 2001; Rudels et al., 2005) (Figure 3b). At about  $79^{\circ}30'$ N a current bifurcates westwards from the YPB and following the northern flank of Molloy Deep re-enters the Greenland Sea through eastern Fram Strait (Figures 2 and 3). A fraction of the YPB is diverted eastwards into the Litke Trough (Figure 2) and another current bifurcates from the YPB at the northeast tip of the plateau continuing east along the lower continental slope of Nansen Basin (Figure 3). Cokelet et al. (2008) obtained 30% higher geostrophic velocities in the SVB north of Svalbard, than in the model. North of Svalbard the SVB and both branches of the YPB merge into the fast ( $0.09 \text{ m s}^{-1}$ ) FSB.

In Fram Strait, the observed depth of the NAW core is at 150-200 m (Cokelet et al., 2008; Furevik et al., 2007; Schauer et al., 2004) in close agreement with the model (175 m). The lower boundary of the NAW ( $\sigma_t=28.0$ ) has been observed at 600 m (Schauer, 1995) or 700 m by Cokelet et al. (2008), and is at 715m in the model. North

of Svalbard the model lower NAW boundary is at 1100 m next to the shelf raising to 500 m offshore; deeper than 950 m and 400 m observed by Cokelet et al. (2008). Further east the NAW layer is capped by the 100-300 m thick layer of the surface and halocline waters. In Fram Strait, the simulated NAW fraction in the KB is colder than in the WSC, whereas the SVB carries slightly warmer NAW than the YPB (Table 3). Overall, the simulated SVB in Fram Strait and north of Svalbard is warmer and more saline than the YPB (Table 4), consistent with observations (Saloranta and Haugan, 2001; Schauer et al., 2004).

### 3.3 *NAW in the Barents and Kara Seas*

Only the upper part of the Atlantic inflow can enter the Barents Sea. The model circulation shows good agreement with the limited current-meter observations (Ingvaldsen et al., 2004a; McClimans et al., 2000; Panteleev et al., 2004; Schauer et al., 2002). In both the NAW enters the Barents Sea as a northern core (NKCN) and southern core (NKCS) of the NKC (Furevik, 2001; Ingvaldsen et al., 2004a). A northern pathway leads from the Bear Island Trough via the Hopen Trench into Hinlopen Basin and then northward between Svalbard and Franz-Josef Land into the Arctic Ocean (Figure 6). Part of the NAW within this pathway flows along the northern flank of Central Bank, enters Eastern Basin, then flows south joining the WNZC (Figure 3b). A southern pathway leads from the Bear Island Trough into Central Basin as the NKCS, along the western flank of the Novaya Zemlya Shelf as the Western Novaya Zemlya Current (WNZC), and between Franz-Josef Land and Novaya Zemlya via the St. Anna Trough into the Arctic Ocean (Figures 3, 7 and 8). The NKCS begins as a slow broad flow, then becomes narrower, faster flowing into the Barents Sea above the 300 m isobath between Central Bank and Nordkapp Bank

and arrives in Central Basin of the Barents Sea (Figures 2b and 3b). Here, the topographically steered cyclonic circulation and cooling creates a doming of the Barents Sea Bottom Water (BBW) forcing NAW into cyclonic circulation with a residence time sufficient for these waters to mix. The result is cooling and freshening of the NAW also observed by Schauer et al. (2002). The modified NAW continues east within the Murman Current, and then, in agreement with observations (Ozhigin et al., 2000), flows north along the 205 m depth contour within the WNZC, arriving in the northeastern Barents Sea. Densification of the NAW occurs through the mixing with cold, brine-enriched dense water produced by cooling and ice formation in the leeward polynyas west of Novaya Zemlya (Schauer et al., 2002; Ivanov and Shapiro, 2005). From the northeastern Barents Sea, NAW flows into the Kara Sea at the southern side of the Franz-Josef Land - Novaya Zemlya passage and enters Nansen Basin on the eastern side of the St. Anna Trough.

In Franz-Josef Land and Novaya Zemlya gap the simulated WNZC has two cores (each is ~30 km wide) above the upper and lower slope of the Novaya Zemlya shelf and has a strong barotropic component and maximum velocities at the bottom ( $0.13 \text{ m s}^{-1}$ , Figure 7). Observations showed similar barotropic structure and velocities (Schauer et al., 2002). In the model, a strong cyclonic vortex appears in the Franz-Josef Land–Novaya Zemlya channel (*ca.*  $60^{\circ}30'E$ ,  $78^{\circ}N$ ) in the top 200 m (Figure 3b), a feature seen in current-meter measurements (Schauer et al., 2002.). The outflow through the St. Anna Trough occurs on the eastern side as a strong barotropic current (0-100m,  $0.14 \text{ m s}^{-1}$ ). Part of the FSB also deviates into the St. Anna Trough along its western slope and re-circulates cyclonically in the St. Anna Trough ( $0.08 \text{ m s}^{-1}$ , Figures 3 and 8), also consistent with observations (Hanzlick and Aagaard, 1980; Schauer et al., 2002). Hanzlick and Aagaard (1980) suggest that some fraction of

NAW may continue southwards along the eastern coast of Novaya Zemlya as a narrow, ~10-20 km, wide current and join the Eastern Novaya Zemlya Current. In the model there is a 16 km wide, weak ( $< 0.01 \text{ m s}^{-1}$ ), southward flow of heavily diluted NAW along the eastern coast of Novaya Zemlya.

In the model the NCC enters the western Barents Sea at approximately as a fast current ( $0.12 \text{ m s}^{-1}$ ) and carries warm, fresh Norwegian Coastal Water with mean-annual temperature and salinity of  $4.8 \pm 1.6^\circ\text{C}$  and  $34.45 \pm 0.05$ , within the range of values given by Loeng (1991) and Schauer et al. (2002). The NCC bounds the NKCS from the south diluting the southernmost fraction of NAW (Figure 9); it follows the northern Norwegian and Russian coasts above 100 m depth up to  $24^\circ\text{E}$ , then it continues along the coast as the Norwegian Murmansk Coastal Current. After absorbing waters from the White Sea, the Norwegian Murmansk Coastal Current turns north-northeast and joins the Novaya Zemlya Coastal Current (NZCC), with a branch leaving the Barents Sea on the southern side of the 80-m deep Kara Gate. In the model and observations (Ozhigin et al., 2000; Ivanov and Shapiro, 2005), the NZCC originates from the cold, fresh Litke Current arriving from the Kara Sea through the Kara Gate; it flows northwards along the western coast of Novaya Zemlya, becoming colder and more saline due to ice formation in the leeward polynyas and enters the gap between Franz-Josef Land and Novaya Zemlya as a ~40 km wide barotropic current above the shelf ( $0.11 \text{ m s}^{-1}$  with mean-annual temperature and salinity from  $-1.9$  to  $-1.0^\circ$  and  $34.20$ - $34.80$ ) (section 14, Figure 7).

A narrow, fast NKC (  $0.08 \text{ m s}^{-1}$  ) separates from the WSC at the northern flank of the Bear Island Trough, diverts southward and flows east above the 400 m depth contour. Part of the NKC continues south along the 300 m depth contour merging

with the NKCS, whereas the main current flows along the 400 m depth contour into the Hopen Trench and then into Hinlopen Basin. From there it enters the Arctic Ocean through the Kvitøya Channel and on the eastern side of the Victoria Channel (Figures 3 and 7). In the Hopen Trench the circulation is cyclonic and the Eastern Current bifurcates into the passage between Stor Bank and Central Bank and then divides into two currents, the first flows into Central Basin and the other towards Franz-Josef Land (Figure 3b). The cyclonic circulation above Central Bank has been seen in observations (Quadfasel et al., 1992). There are no direct current-meter measurements to validate the pathways of the EC in the model, but inverse modelling shows the eastward flow between Stor Bank and Central Bank, in agreement with our results (Panteleev et al., 2004). The remaining part of the NKCN returns back to the Norwegian Sea along the northern slopes of the Hopen Trench and Bear Island Trough as a barotropic, topographically guided current. At the entrance of the trough, part of the current continues north along the western Spitsbergen Shelf and part joins the northern branch of the NKC, closing the re-circulation (Figures 3 and 9), in agreement with current-meter measurements (e.g. Ingvaldsen et al., 2004a). The eastward current (width ~60 km,  $0.05 \text{ m s}^{-1}$ ) was identified as a retrograde slope jet (Slagstad and McClimans; 2005) and flows above the southern flank of Bjørnøya Bank, bringing modified NAW (0-2°C and 34.6-34.85) NAW into the western Barents Sea (Figure 9b). The jet in the present model is weak compared to the large inflow in the regional Barents Sea Model of Slagstad and McClimans (2005).

Polar Surface Water (PSW) (-1.0 to 3.0°C, and 32.00-34.00) and Polar Intermediate Water (PIW) (-1.8 to -1.0°C, 34.30-34.70) advected from the Arctic Ocean into the northern Barents Sea (Figure 3b) are found in the model in the upper 80 m of the water column, which is in agreement with observations (Pfirman et al., 1994). These

water masses spread southwards through the Barents Sea by the Perseus Current, the Hopen-Bjørnøya Current and the Bear Island Current, forming the Barents Sea Polar Front with NAW and contributing to the West Spitsbergen Coastal Current.

In transit through the Barents and Kara Seas, NAW rapidly cools and freshens due to mixing with polar and coastal waters, atmospheric precipitation and sea ice melting.

In the western part of the Barents Sea the NAW within the NKCN has average temperature and salinity of  $5.2 \pm 1.2^\circ\text{C}$  and  $35.03 \pm 0.02$ , and is colder and more saline than in the NKCS ( $6.1^\circ\text{C}$  and  $34.97$ ); whereas the NAW outflow through the Victoria Channel has average temperature and salinity of  $1.3 \pm 0.6^\circ\text{C}$  and  $34.89 \pm 0.02$ . In the channel between Franz-Josef Land and Novaya Zemlya warm NAW is absent; here only the dense fraction of NAW with average temperature and salinity of  $-0.2 \pm 0.4^\circ\text{C}$  and  $34.81 \pm 0.01$  is present; no NAW appears in the Voronin Trough. Therefore, the model supports observational results that after having been transformed in the Barents Sea, the warm temperature signal of NAW is completely lost (Schauer et al., 2002).

### 3.4 *Oceanic transports*

Oceanic transports characterise the impact of the NAW inflow on the Arctic Ocean. In the Nordic Seas, transports of volume, heat and salt in the SC and FC are almost equal, with the simulated NAW inflow across the Greenland-Scotland Ridge *ca.* 10% weaker than is observed (Table 2). Farther north, within the Norwegian Atlantic Current, the model NAW transport is equally divided between the western and eastern branches of the current, in agreement with observations (Orvik et al., 2001; Orvik and Skagseth, 2005). The total simulated NAW transport in the Norwegian Atlantic Current of 5.2–6.5 Sv is typically within  $\pm 10\%$  of the estimates obtained from geostrophic calculations and current meter moorings (Table 1). However, for the

inflow across Iceland-Faroe Ridge and through Denmark Strait the differences are  $\pm 18\%$  and  $\pm 20\%$  because more of the simulated NAW inflow diverts into Denmark Strait reducing the northward flow of NAW between Iceland and Faroe Islands. The total simulated NAW inflow between Greenland and Faroe Islands is 11% weaker than the observed (Table 2).

In Fram Strait the WSC (initially  $3.4 \pm 1.5$  Sv strong) loses one-third of the flow and associated heat and salt to the KB; the remaining flow enters Fram Strait (Table 4). The large variability of the mean simulated flow in the KB is a consequence of the semi-permanent stationary meandering current over the northernmost tip of the Knipovich Ridge, also detected in current meter data (Schauer et al., 2004). Estimates from extensive current meter observations in Fram Strait at  $79^\circ\text{N}$  gave total volume transports within the WSC of  $3.1 \pm 1.0$  Sv and  $4.0 \pm 1.0$  Sv northwards and quasi-heat transports of  $28 \pm 5$  TW and  $44 \pm 6$  TW northwards (Fahrbach et al., 2001). The corresponding model transports for these years are  $1.9 \pm 1.2$  Sv and  $2.8 \pm 1.2$  Sv, and  $23 \pm 15$  TW and  $36 \pm 16$  TW, a reasonable agreement.

In the western Barents Sea, the simulated net total transport of  $2.2 \pm 0.8$  Sv (Table 4) through the Fugløy-Bjørnøya hydrographic section (section 8, Figure 3b) agrees well with the transport of 1.3-2.0 Sv from current meter measurements (Ingvaldsen et al., 2004a). The total simulated inflow of NAW into the western Barents Sea between Fugløy and Bjørnøya is  $3.0 \pm 0.8$  Sv, and the re-circulation of NAW into the Norwegian Sea is  $1.2 \pm 0.7$  Sv. These figures agree with estimates from Blindheim (1989), which include a fraction of BBW flowing westward, given as  $0.2 \pm 0.1$  Sv in the model. The simulated total quasi-heat transport into the western Barents Sea (Table 4) is in reasonable agreement with the 62-82 TW for 1970-1990 (Simonsen

and Haugan, 1996), and the simulated NAW transport (Table 3) agrees within 8% with another estimate of 48 TW (Skagseth et al., 2008).

In the model the main outflow from the Barents Sea is into the St. Anna Trough,  $1.4 \pm 0.6$  Sv (section 13, Figure 3b) in agreement with the estimates of  $1.5 \pm 0.5$  Sv by Loeng et al. (1997) and Schauer et al. (2002). The simulated outflows between Svalbard and Franz-Josef Land and through the Kara Gate (sections 12 and 14, Figure 3b) are smaller (Tables 4 and 5) with NAW contributing half the flow (Table 4). The NAW outflow into the Arctic Ocean through the Victoria Channel is  $0.3 \pm 0.1$  Sv. The net volume, heat and salt transports through the St. Anna Trough (section 15, Figure 3b) are equal to the transports from the Barents Sea into the Kara Sea (Table 5). The net outflow through the Voronin Trough (section 16, Figure 3b) into the Arctic Ocean is  $0.2 \pm 0.1$  Sv and is balanced by the flows through the Kara Gate, Wilkitsky and Shokalsky straits (Table 5), and by precipitation and evaporation in the Kara Sea. There is almost no exchange between flows through the St. Anna Trough and through the Voronin Trough. The volume and salt transport from the Barents and Kara Seas into Nansen Basin ( $2.0 \pm 0.7$  Sv northwards, and  $70 \pm 19$  k·Ts<sup>-1</sup> northwards) are about two-thirds of the transports through Fram Strait (Table 4). The corresponding quasi-heat transport of  $7 \pm 2$  TW southwards is small compared to the heat coming through the strait: thus, the Arctic Ocean gains heat from the FSB and loses it to the BSB.

There are few observational estimates of the transports across the northern shelves of the Barents and Kara Seas. An inflow of 0.3-0.4 Sv from the Arctic Ocean into the northern Barents Sea, and outflow of 0.1 Sv into the Arctic Ocean were deduced from volume conservation arguments, from regional modelling and data assimilation (Loeng et al., 1997; Maslowski et al., 2004; Panteleev et al., 2007). The observed net

volume transport through the St. Anna Trough is 0.6-1.2 Sv northwards and the quasi-heat transport is between 4 TW southwards and 4 TW northwards (Simonsen and Haugan, 1996). The model transports are within the range of observations (Table 5). The total net volume, heat (referenced to  $-0.1^{\circ}\text{C}$ ) and total salt transports from the Barents and Kara Seas into Nansen Basin obtained from a regional high-resolution model (Maslowski et al., 2004) are 2.3 Sv northwards, 2 TW southwards, and  $77 \text{ kT}\cdot\text{s}^{-1}$  northwards, which is close to our results.

### ***3.5 Mixed Layers and Sea Ice***

The mean-annual mixed layer depth defined in the model as the average of the maximum depth of the daily mixing calculated by the KPP scheme shows the correct spatial structure and agrees well with the mixed layer depth obtained from the World Ocean Atlas Climatology (National Oceanic and Atmospheric Administration, <http://www.cdc.noaa.gov/>): both show steep deepening of the mixed layer in the Greenland Sea and western Barents Sea, an increase in the mixed layer depth in Central Basin of the Barents Sea, and a decrease in the mixed layer depth north of the Barents Sea Polar Front, in the southern Barents Sea and in the Kara Sea (Figure 10).

Sea ice participates in the formation of the upper halocline waters in the Barents and Kara Seas, so the performance of the sea ice model in these areas is relevant to the NAW transformation. Comparisons between simulations and data from the Special Sensor Microwave/ Imager (SSM/I) (Comiso, 1999) demonstrate that the sea ice model performs well: the simulated total winter ice extent in the Barents Sea agrees to within 3% of the observations and the simulated total mean-annual ice extent is within 5% agreement. The modelled and observed distribution of the sea ice fraction (not shown) also in reasonable agreement, although there is an excess of sea ice in the

Kara Sea in summer (Comiso, 1999). The simulated ice flux through Fram Strait agrees within 2% (Kwok et al., 2004).

### 3.6 *Summary of model evaluation*

The model presents a consistent picture of the NAW inflow in the Arctic Ocean and allows us to resolve details of the NAW circulation not resolved in other coarser resolution models. Where observations exist the model is consistent with them, so we conclude that model performs adequately to study the NAW circulation. The main evidence for this assertion is summarised as follows: Model volume and total salt transports are within  $\pm 20\%$  of the observational estimates. Temperature and salinity of the NAW flow through the Nordic Seas are in good agreement with observations. The depth range of the inflow is accurate within 13%. The upper-ocean horizontal circulation in the model is reasonable: the mean surface ocean currents agree with circulation derived from drifters. The mixed layer representation, including winter convection is realistic. The formation of sea-ice is realistic.

The simulated convection in shallow (approximately hundreds of metres) water is realistic. The model representation of deep convection is questionable, but is not significant for this study since the deep circulation is not addressed. Therefore, there is sufficient agreement between the model results and the observations to suggest the model has enough predictive skills to justify using the results to describe circulation features between observational sections and for expanding the analysis into areas where observations are scarce: the northern Barents Sea and the Arctic Ocean.

Since the model here has a higher resolution than any of the global OGCMs (to the best of authors' knowledge, the only existing  $1/12^\circ$  global model suitable for inter-decadal studies is the Parallel Ocean Program (POP) global model with no results

publicly available), and few regional models at the same resolution currently exist (Maslowski et al., 2004; Slagstad and McClimans, 2005) the comparison with other models presents a challenge. The closest to our model set-up with respect to the model physics is the regional Arctic model described in Maslowski et al. (2004). This model shows a similar type of the circulation in the Barents Sea as our model does, but the simulated inflow into the western Barents Sea in this model is stronger than in our results. This is possibly due to the higher Ekman transport caused by the stronger southerly component in the near-surface wind field (Ingvaldsen et al., 2004b) from the reanalysis ERA-15 of the European Centre for Medium-Range Weather Forecasting (ECMWF) in comparison to that from NCEP (e.g. Bromwich and Wang, 2005). Slagstad and McClimans (2005) presented the results from a 4-km resolution regional model of the Barents Sea nested in a 20-km resolution model of the Nordic Sea and demonstrated agreement with observed thermo-haline properties on the Norway to Svalbard section. However their simulated inflow into the western Barents Sea is too weak compare to a current-meter data. Karcher and Oberhuber (2002), integrating a 50-km resolution regional Arctic-North Atlantic isopycnic model forced with the ECMWF –derived climatology, obtained realistic flow through the Barents Sea, however the inflow through Fram Strait is half of the observed. A variety of Arctic Ocean simulations were carried out within Arctic Ocean Model Intercomparison Project (AOMIP) (Proshutinsky and Kowalik, 2007). Olsen and Schmith (2007) performed ensemble-hindcast simulations for the period 1948-2005 with a global coupled sea ice-ocean model with resolution up to 20-km in the Arctic and obtained realistic transports across Greenland-Scotland Ridge, but the NAW inflow in Fram Strait (1.3 Sv) in their simulations is half the strength of the observations and our model results. In general, coarser resolution models tend to underestimate NAW

inflow through Fram Strait unless alteration of the model bathymetry is applied, whereas the high resolution models (global and regional) give more realistic results provided realistic atmospheric forcing and lateral boundary conditions (for regional models) are used. Because only limited observations of the near-surface wind in the area are available, it is impossible to conclude whether biases in simulated oceanic transports in Fram Strait and the western Barents Sea are due to deficiency in forcing fields or due to model physics.

#### **4. Discussion**

##### **4.1 Transformation of NAW in the Barents and Kara Seas**

A variety of mechanisms modify the NAW in the Barents and Kara Seas.

Densification of the water column due to atmospheric cooling and ice formation, and its dilution due to atmospheric precipitation, ice melting and mixing with surface and coastal waters result in segregation of the NAW into Cold Halocline Water (CHW), Cold Deep Water (CDW), and bottom waters, all of them are colder than NAW. CHW is formed by atmospheric cooling of NAW and subsequent modification due to ice melting at the Marginal Ice Zone of the northern Barents Sea (Steele et al., 1995); the CDW is formed by NAW cooling at the Marginal Ice Zone and is denser than CHW (Steele et al., 1995). Both CHW and CDW are lighter than the NAW but heavier than the surface waters; they are subducted under the surface waters and flow northwards and eastward (Steele et al., 1995). Following Midttun (1985), convection in the Barents Sea happens in two stages: first the upper ocean layer cools to the freezing temperature and its density increases, leading to the deepening of the upper cold low salinity layer (step 1), then brine rejection due to sea ice formation sets haline convection (step 2). If the water column is weakly stratified and the ice

formation rate is high, convection may reach the seabed; otherwise it extends to some intermediate depths.

Analysing the simulated density structure we found several places of intermediate-depth convection, where the water column is weakly stratified above the penetration depth and has strong stratification below this level. The deepening of the mixed layer and increased level of the ventilation tracer down to convective depth have also confirmed the convection at these sites. The principal site is in the Franz-Josef Land–Novaya Zemlya channel ( $78^{\circ}\text{N}$ ,  $60^{\circ}30'\text{E}$ ) (Figure 10, site n4). A smaller convective site is located in Hinlopen Basin southeast from Svalbard ( $78^{\circ}\text{N}$ ,  $28^{\circ}\text{E}$ ) (site s3), where the plume of cold ( $-1.8^{\circ}\text{C}$ ) and relatively fresh (34.00) water extends from the surface to a depth of 52 m. Below this depth, temperature, salinity, and density increase, and the water column is strongly stratified. In the simulated temperature field at a depth of 120 m this plume manifests itself as a patch of very cold water next to the eastern flank of Spitsbergen Bank (Figure 3b), coincident with the winter coastal polynya, which has been speculated to be a source for water densification (Vinje and Kvambekk, 1991). The simulations show two other shallow convective sites east of Stor Bank (site c5) and east of Franz-Josef Land ( $80^{\circ}40'\text{N}$ ,  $59^{\circ}20'\text{E}$ ) (site f2). All three convective sites produce CHW and are located in the areas of recurring winter sea ice cover that limits the convective depth (the mean-annual minimum sea ice extent is shown in Figure 10). However the ice divergence constantly reduces ice fraction causing ice to form in the open water leads and ice grows from the underside of the ice, thus, the sea ice formation rate is high and produces salt in sufficient quantity to initiate convection in the weakly stratified water column, the latter occurs due to the preconditioning, discussed below.

Figure 10 shows the sites where in the model full-depth convection occurs. The principal area is in Central Basin (sites c1, c2 and c4), and other sites are in Storfjord (78°N, 20°E) (site s2), and at Spitsbergen Bank (site s1), southeast of Central Bank (74°45'N, 38°30'E) (site c3), west of Novaya Zemlya (75°30'N, 56°E) (sites n1 and n2) and west of Franz-Josef Land (80°40'N, 49°E) (site f1). At these sites cold water (from -1.8 to -0.5°C) with salinity of 34.63-35.02 occupies the full-depth; the mixed layer extends down to the bottom, and the stratification is weak and the ventilation tracer level is high through the whole water column. These sites produce BBW, and are essentially the areas with low sea ice fraction in winter (Figures 10 and 11), which enhances ice production and brine-enriched water formation, the mechanism discussed for example by Ivanov and Shapiro (2005). Dense water formation at sites s2, c3 and f1 has been observed, suggesting that convection occurs at these sites (e.g. Ivanov et al., 2004; Quadfasel et al., 1992; Schauer and Fahrbach, 1999). In the model, the dense water formed at sites c3, s2 and s1 flows west contributing to the intermediate and deep waters of the Norwegian and Greenland Seas and enters Nansen Basin as a lower part of the inflow; this is confirmed by observations (Schauer and Fahrbach, 1999; Ivanov et al., 2004). The ocean convection is very difficult to observe, as it is the intermittent process with the relatively small horizontal scale of the convective plumes. Despite that, the large number of successful direct measurements of the vertical velocity in the convective areas has been made using neutral buoyancy drifters in Gulf of Lions and Labrador Seas (for the overview see e.g. Marshall and Schott, 1999). In addition, the ventilation tracers such as O<sup>18</sup> and density structure show the areas of the sinking water. The high-resolution modelling studies (e.g. Ivanov et al., 2007) show the good correspondence between the density structure detected from the CTD measurements and simulated sinking of the water in

the convection plumes. Therefore, the convection events can be detected with high degree of confidence.

In Central Basin simulated full-depth convection occurs at three separate locations: at  $75^{\circ}30'N$ ,  $43^{\circ}E$  and at  $73^{\circ}45'N$ ,  $43^{\circ}45'E$ , and at  $71^{\circ}30'N$ ,  $30^{\circ}E$  (Figure 10, sites c1, c2 and c4). The first site has been discussed in the literature (e.g. Schauer et al., 2002); the others have not been reported before. In addition full-depth convection occurs in the seabed depression at  $77^{\circ}N$ ,  $50^{\circ}45'E$  (Figure 10, site n3). This site is different: cold CDW spreads over the whole depression area with a fraction flowing across the sill between Franz-Josef Land and Novaya Zemlya.

Most of the convective sites, detected in the model, appear every winter at the same locations with some variation in the depth of the mixed layer from year to year. Figure 11 depicts the simulated maximum mixed layer depth in March 1989, the year characterised by the centennial maximum winter (December-March) North Atlantic Oscillation index (NAO) (<http://www.cgd.ucar.edu/cas/jhurrell/nao.stat.winter.html>), in March 1995 (positive winter NAO index) and March 2001 (negative winter NAO index) along with timeseries of the maximum monthly mean mixed layer depth for the period of analysis (Figure 11a,b,c). The latter were obtained at convective sites by averaging over 121 model cells in the fixed location for each site. We have analysed model monthly mean fields 1989-2004 (not shown) to make sure that the convective sites are the localised spots of the deep mixed layer with associated weak stratification, and not just a homogeneous deepening of the winter mixed layer. We used a ventilation tracer to detect the ventilation of the water column at the simulated convection sites. Several conclusions can be made. First, we see the robust seasonal cycle with maximum mixed layer depth in February-March at all sites (Figure 11d).

Secondly, convection happens practically at the same locations every year, however the strength of convection varies. There is interplay between deep convective sites in the western Barents Sea (site s1 on the figure) and in the Central basin of the Barents Sea (sites c1, c2 and c4 on the figure). Convection at site s1, prominent in 1990s, in 2001-2004 underwent a spectacular weakening, but is still present at the same location (Figure 11). We believe the reason for the variability is the atmospheric fresh water forcing, however the analysis of the variability is beyond the scope of this paper. Finally, the intermediate-depth convective sites c5 and s3, and the site n4 in the St. Anna Trough are remarkably persistent in the model. The intermediate-depth convective sites are associated with vertical homogenisation of the water column by the circulation around bathymetric features (e.g. Marshall and Schott, 1999). Quadfasel et al. (1992) discussed the preconditioning of the convection in the vicinity of Central Bank in the western Barents Sea through the Taylor column effect. The preconditioning by the stable topographic currents gives a plausible hypothesis to explain why the shelf convection in the Barents Sea persists at the same sites from year to year.

In the simulation the outflow of the modified waters of the Barents Sea into the Arctic Ocean occurs mainly through the Franz-Josef-Novaya Zemlya passage and then through the St. Anna Trough and consists of saline BBW and two types of the lighter halocline waters, CHW and CDW, which make a major contribution to the outflow (Figure 3, hydrographic sections 13 and 15; Figures 7 and 8). Based on hydrographic sections Schauer et al. (2002) concluded that two modes constitute the Barents Sea outflow through the St. Anna Trough: the relatively warm (*ca.*  $-0.5^{\circ}\text{C}$ ), saline (*ca.* 34.85) BBW in the central part of the trough, which could be traced back to NAW modification in Central Basin of the Barents Sea and the cold (*ca.*  $-1.3^{\circ}\text{C}$ ), low

salinity (*ca.* 34.75) water at the upper part of the flank of unknown origin. Our simulation suggests that the cold mode of the outflow is CHW and offers an explanation of how it is produced. The CHW is formed through intermediate-depth convection west of the Franz-Josef Land–Novaya Zemlya passage (Figure 10, site n4) from the northern Barents Sea halocline waters advected into the St. Anna Trough by two currents flowing north and south of Franz-Josef Land, and from PSW and PIW entering from the Arctic Ocean (Figures 3b and 7): the upper ocean layer first cools to the freezing temperature and its density increases, leading to the deepening of the upper cold, low salinity layer (step 1, according to Midttun, 1985). Since the area is covered by sea ice advected from the Arctic Ocean and the ice formation is limited, haline convection (step 2) does not develop fully and the CHW sinks only to a depth of *ca.* 170 m descending into the St. Anna Trough. The depression in the haline surfaces (and freshening of the 100-170 m-deep layer) caused by the CHW formation is evident in both model results (section 13, Figure 7) and observations (Midttun, 1985; Schauer et al., 2002). The horizontal density gradient between CHW and water within WNZC combined with topographic steering of the flow through the Franz-Josef Land–Novaya Zemlya passage results in the bottom intensified cyclonic vortex in the channel (Figure 3b). It is worth mentioning that other high-resolution models show the topographically-steered currents and structure of the mixed layer similar to ours (e.g. Maslowski et al., 2004; Slagstad et al., 2005), this suggests that the results we discuss in the paper are model-independent.

Using the technique described in Speer (1993), which links the formation rates of water in  $T$ – $S$  classes to surface heat and freshwater forcing and subsurface mixing, we calculated formation rates of NAW and halocline waters with  $T < 0^{\circ}\text{C}$  and  $S < 34.8$  (representing CHW and CDW). The surface heat also included the atmospheric heat

of sea ice formation. The freshwater forcing included precipitation, evaporation, sea ice and snow melt and the restoring term. From the balance of the transformation rates and ocean advection we estimate the rate of modification of the water masses through mixing. The calculations for three closed regions in the Barents Sea: northern region, St. Anna Trough and southern region (areas III, IIIa, and IV, Figure 12) show that the decrease of the NAW volume occurs in all areas of the sea through mixing; the production of NAW in the southern Barents Sea due to surface forcing is not large enough to compensate for the loss (Table 6). The NAW transformation rate through mixing is uniform through the sea and is reduced in St. Anna Trough. Atmospheric cooling is the principal mechanism for halocline water production in all areas of the Barents Sea; there is a small gain of the halocline waters through mixing in St Anna Trough (Table 6). The trough is an important source of the halocline waters: the intensity of transformation (rate of transformation per unit area) is as high as in the northern region of the Barents Sea.

#### **4.2 Branches of the NAW inflow**

Overall, *ca.* 2.1 Sv, i.e. less than half of the 6.9 Sv of the NAW entering the Nordic Seas across the Greenland-Scotland Ridge, reaches the Arctic Ocean relatively unmodified within the FSB; *ca.* 3.1 Sv of NAW is re-circulated and modified in the Nordic Seas and returns into the North Atlantic. The remaining part of the NAW inflow, *ca.* 1.7 Sv, progresses as the BSB through the Barents and Kara Seas, where it is transformed into mode waters. In the model, the NAW share of the heat flux through the eastern Fram Strait into the Arctic is about half that through the western Barents Sea, a fact acknowledged by other models and observations (e.g. Maslowski et al., 2004; Schauer et al., 2002); but only 10% of the heat coming from the

Norwegian Sea into the western Barents Sea reaches the Arctic. The salt fluxes associated with NAW within the FSB and within the BSB are comparable.

We have calculated the heat and salt balances for the Nordic Seas, Barents and Kara Seas by taking differences between simulated transports across the sections that fully enclose these regions in the model: the Greenland-Scotland Ridge, a section between Scotland and Norway, Fram Strait, Svalbard-Norway, Svalbard-Severnaya Zemlya, and the Kara Gate, Shokalsky and Wilkitsky straits. The use of the closed regions allowed us to obtain ‘true’ heat balance as the volume transports vanish to zero (we took into account sea ice and snow transports and variation in sea surface height due to atmospheric fresh water in the calculations). We calculated surface heat and “salinity” forcing; the latter has been obtained from the total surface freshwater flux including atmospheric fluxes, sea ice and snow melt and the restoring term. The main heat and salt loss of the NAW occurs in the Nordic Seas (140 TW and 71 kT/s); atmospheric fluxes drive most of the cooling (122 TW) with the remaining heat loss due to mixing. In the model the freshening due to the surface flux is small (3 kT/s in salt equivalent) and mixing contributes the remaining 69 kT/s of NAW freshening; similarly in the Barents Sea: the surface fresh water contributes only 2 kT/s into the total salt loss of 62 kT/s. However, in contrast to the Nordic Seas, only 26 TW of 61 TW of the surface heat flux in the Barents Sea are used for the NAW cooling, the remaining flux is used for the halocline water formation, consistent with the water mass formation discussed earlier in section 4.1.

The route through Fram Strait provides the Arctic Ocean with two types of NAW: the warmer and more saline NAW confined to the shallow coastal SVB, and the intermediate depth NAW, transported within the YPB. East of the Yermak Plateau the

SVB joins the YPB and forms the eastward-flowing FSB (Figure 3b). Three main channels are available for the NAW outflow from the Barents Sea into Nansen Basin: the passage between Svalbard and Franz-Josef Land, St. Anna Trough and Voronin Trough. The first portion of the BSB leaves the Barents Sea via the eastern Victoria Channel as a narrow current with the main part of BSB flowing through the St. Anna Trough, where the halocline waters (CHW and CDW) form the fast current along the upper part of the eastern flank of the channel (Figures 3 and 8). Further on, this current turns eastwards and follows the Siberian shelf break as a shallow current (mean-annual velocity up to  $0.11 \text{ m s}^{-1}$ ) above the continental shelf break at depths of 50-200 m (Figure 3). BBW enters Nansen Basin along the lower part of the eastern flank of the St. Anna Trough (Figure 8), sinks to about 900 m and continues eastward with the core of  $0.08 \text{ m s}^{-1}$  above the upper part of the continental shelf slope. Both the halocline water core and the BBW cores form part of the Arctic Ocean Boundary Current and further downstream they merge into a single upper-slope current with two almost undistinguishable cores, which however maintains the distinct thermo-haline properties of the Barents Sea mode waters CHW and CDW and BBW. Intrusion of the Barents Sea waters into Nansen Basin via the Victoria Channel and St. Anna Trough displaces the core of the FSB offshore, away from the continental shelf slope (Figure 3b) and downwards; this effect has been observed in hydrographic sections (Schauer et al., 1997).

Within the Arctic Ocean Boundary Current the FSB transports  $1.2 \text{ Sv}$  of warm, saline NAW, whereas the BSB carries  $0.4 \text{ Sv}$  of BBW and  $0.9 \text{ Sv}$  of halocline waters, making the total BSB contribution greater than that of the FSB. The FSB and the BSB carry roughly equal amounts of salt:  $46 \text{ kT}\cdot\text{s}^{-1}$  and  $44 \text{ kT}\cdot\text{s}^{-1}$ , with halocline waters contributing  $12 \text{ kT}\cdot\text{s}^{-1}$  and BBW contribution of  $32 \text{ kT}\cdot\text{s}^{-1}$ . North of the St. Anna

Trough part of the FSB (*ca.* 0.7 Sv) is diverted into the interior of Nansen Basin with the rest of it continuing along the foot of the shelf slope. Although the outflow through the St. Anna Trough dominates, the outflow through the Svalbard to Franz-Josef Land passage contributes about 20% to the total salt flux within the BSB.

#### **4.3 Revised scheme of the NAW inflow**

In this section we describe a revised schematic of the NAW inflow into the Arctic Ocean, which is derived from our model and supported by available observations. Four areas of the NAW inflow can be identified (I, II, III together with IIIa and IV in Figure 12). In the area I, which includes the southern Bear Island Trough and Nordkapp Bank, the Norwegian Atlantic Current divides into the WSC and NKC. Area II includes the northern Bear Island Trough, the eastern Fram Strait, Svalbard and Yermak Plateau, where the warm FSB dominates the inflow, and where the NAW is least modified. Area III includes Hopen Trench, north-western Barents Sea, Kvitøya Island, Victoria Channel, Franz-Josef Land, and also the north-eastern Barents Sea; area IIIa includes St. Anna Trough. In this area the contribution of the BSB is significant and NAW undergoes moderate cooling, and cold and fresh halocline waters are produced. This is also the area where the interaction between the FSB and BSB occurs. Area IV is characterised by strong modification of NAW within the BSB through atmospheric cooling, mixing with cascading brine-enriched waters, and through interaction with coastal and shelf waters. This is where saline BBW is produced. The area includes Central Bank, Central Basin and western Novaya Zemlya shelf.

The NAW circulation in the Barents Sea consists of many narrow, topographically steered currents (Figure 3b). From the Barents Sea NAW is delivered to the Arctic

Ocean by two branches. The northern branch flows through areas III and IIIa, with the main fraction of NAW leaving the Barents Sea through the Victoria Channel, following the northern and eastern flanks of the Franz-Josef Land shelf and entering the St. Anna Trough. The remaining NAW within the northern branch flows westward within the EC and then south of Franz-Josef Land into the St. Anna Trough, merging with the main part of the branch. The northern branch, which we call the Franz-Josef Land Branch (FJB), circulates cyclonically in the St. Anna Trough and finally enters Nansen Basin. This branch delivers NAW from the western Barents Sea, mixed to some extent with the FSB that has entered the Barents Sea from the north between Svalbard and Franz-Josef Land and through the St. Anna Trough (Figure 12). Following the northern shelf of Franz-Josef Land, the waters of the branch interact with cold, saline waters produced in the convective site near Franz-Josef Land (marked as f1 in Figure 12). The FJB also carries a large volume of the cold halocline waters CHW and CDW formed in the shallow convective sites s3 in Hinlopen Basin, c5 east of Stor Bank and n4 in the Franz-Josef Land- Novaya Zemlya channel, and in the full-depth convective site n3 west of Novaya Zemlya. The southern branch includes the WNZC and flows through area IV into the St. Anna Trough and further into Nansen Basin. We call this the Novaya Zemlya Branch (NZB). This branch supplies the Arctic Ocean with BBW formed at the sites in Central Basin (c1, c2, and c4) and west of Novaya Zemlya (n1 and n2) of the Barents Sea. All three branches, FSB, FJB and NZB, form the core of the eastward-going Arctic Ocean Boundary Current, which follows the Siberian Shelf break to the Lomonosov Ridge (Figure 12).

## 5. *Conclusions*

To investigate the inflow of NAW into the Arctic Ocean we use a global coupled sea ice-ocean model at high resolution. Three pathways of NAW into the Eurasian Arctic have been identified: one leads through Fram Strait and delivers warm and saline NAW into Nansen Basin, the other two follow through the Barents Sea bringing cooled and freshened NAW into the St Anna Trough and further into Nansen Basin. We cannot confirm a clear-cut separation of the NwACE into the WSC and NKC; instead in the model it happens over a large area of the Norwegian shelf and in the western Barents Sea. In Fram Strait the NAW inflow splits into a deeper fraction flowing cyclonically around the Yermak Plateau and a shallow part following the shelf break of Svalbard, merging east of the Yermak Plateau into a single FSB. The flow of NAW through the Barents Sea divides in the vicinity of Central Bank into two large-scale branches, FJB and NZB, which continue separately through the Barents Sea and flow into Nansen Basin through the St. Anna Trough. These routes bring two distinctive mode waters: cold and fresh halocline waters and warmer and more saline BBW. The impact of the NAW segregation due to different types of convection in the Barents Sea is evident downstream in the Arctic Ocean Boundary Current. Analysis of the model results in the Barents Sea reveals two types of convection: shallow and full depth convection. Halocline waters are formed as a result of the interaction between NAW and waters produced at the shallow convective sites in the northern Barents Sea. BBW is a product of the mixing between NAW and dense water produced at the convective site in the south-eastern Barents Sea. Both water masses enter the Eurasian Arctic through the St Anna Trough.

The simulation demonstrates that during the period 1989-2004 the Fram Strait route supplied the Arctic Ocean with about half of the NAW, and with half of the salt and almost all the heat related to the NAW inflow. The remaining half of the NAW has

been modified in the Barents Sea. The FJB contributed twice as much as the NZB; this makes it the principal pathways for the inflow. Overall less than half of the NAW that entered the Nordic Seas across the Greenland-Scotland Ridge reached the Eurasian Arctic Ocean unmodified; large NAW fraction re-circulated into the North Atlantic and the rest of it was modified in the Barents and Kara Seas.

The model has shown itself as a useful tool for obtaining realistic circulation and water mass structures, that can inform the planning of synoptic scale observational programmes in inaccessible areas such as the Arctic Ocean. However, following Holloway and Proshutinsky (2007), future generations of the ocean models should include tides in order to improve simulations in the Arctic Ocean. We consider the research presented here as a step towards drawing a physically based picture and is such, is helping towards gaining a comprehensive understanding of the mechanisms that drive ocean climate change.

### *Acknowledgements*

We would like to express our gratitude to Mrs Beverly de Cuevas and Dr Penny Holliday for their valuable comments on the manuscript. We also wish to thank Mrs Beverly de Cuevas for the help with the model data processing. This research has been completed thanks to the support from RAPID Climate Change Programme and Arctic Synoptic Basin-wide Oceanography Consortium, Natural Environment Research Council (NERC), UK.

*Appendix. List of abbreviations*

Name	Abbreviation
Arctic Ocean Boundary Current	AOBC
Barents Sea Bottom Water	BBW
Barents Sea Branch	BSB
Bear Island Current	BIC
Cold Deep Water	CDW
Cold Halocline Water	CHW
East Greenland Current	EGC
East Spitsbergen Current	ESC
Eastern Novaya Zemlya Current	ENZC
Eurasian Basin Deep Water	EBDW
Faroe Current	FC
Fram Strait Branch	FSB
Franz-Josef Land Branch	FJB
Greenland Sea Gyre	GSG
Greenland-Spitsbergen Sill	GSS
Hopen-Bjørnøya Current	HBC
Knipovich Re-circulation Branch	KB
Molloy Deep Re-circulation Branch	MDB
Murman Current	MC
Nordkapp Current	NKC
Nordkapp Current, northern core	NKCN
Nordkapp Current, southern core	NKCS
North Atlantic Water	NAW
North Icelandic Irminger Current	NIIC
Norwegian Atlantic Current, eastern branch	NwACE
Norwegian Atlantic Current, western branch	NwACW
Norwegian Coastal Current	NCC
Norwegian Coastal Water	NCW
Norwegian Murmansk Coastal Current	NMCC
Norwegian Sea Arctic Intermediate Water	NSAIW
Norwegian Sea Deep Water	NSDW
Novaya Zemlya Branch	NZB
Novaya Zemlya Coastal Current	NZCC
Novaya Zemlya Coastal Water	NZCW
Polar Intermediate Water	PIW
Polar Surface Water	PSW
Shetland Current	SC
Svalbard Branch	SVB
West Spitsbergen Coastal Current	WSSC
West Spitsbergen Current	WSC
West Spitsbergen Current, western core	WSCw
Western Novaya Zemlya Current	WNZC
Yermak Plateau Branch	YPB

## References

- Aagaard, K., Carmack, E.C., 1994. The Arctic and Climate: A Perspective. In: Johannessen, O.M., Muench, R.D., Overland, J.E. (Eds.), *The Polar Oceans and their Role in Shaping the Global Environment*. Geophys. Monogr. Ser., Vol. 85. American Geophys. Union, Washington, pp. 5-20.
- Aagaard, K., Greisman, P., 1975. Towards new mass and heat budgets for the Arctic Ocean. *J. Geophys. Res.* 80, 3821–3827.
- Aksenov, Ye., 2002. The sea ice-ocean global coupled model, ARCICE Project Report Part I: dynamical-thermodynamical sea ice model. Southampton Oceanography Centre Research and Consultancy Report 103, 83 pp.
- Antonov, J.I., Levitus, S., Boyer, T.P., Conkright, M.E., O'Brien, T.D., Stephens, C., 1998. *World Ocean Atlas 1998 Vol. 1: Temperature of the Atlantic Ocean*. NOAA Atlas NESDIS 27, U.S. Government Printing Office, Washington, D.C.
- Barry, R.G., Serreze, M.C., 2000. Atmospheric components of the Arctic Ocean freshwater balance and their interannual variability. In: Lewis, E.L. (Ed.), Jones, E.P., Lemke P., Prose, T.D., Wadhams, P. (Associated Eds.), *The Freshwater Budget of the Arctic Ocean*, NATO Science Series 2, Environment Security, Vol. 70. Kluwer Academic Publishers, Dordrecht, The Netherlands, pp. 45-56.
- Bishop, J.K.B, Rossow, W.B., 1991. Spatial and temporal variability of global solar irradiance. *J. Geophys. Res.* 96, 16839-16858.
- Blindheim J., 1989. Cascading of the Barents Sea bottom water into the Norwegian Sea. *Rapp. P.-V. Reun. Cons. Int. Explor. Mer* 188, 49-58.
- Blindheim, J., Østerhus, S., 2005. The Nordic Seas, main oceanographic features. In: Drange, H., Dokken, T., Furevik, T., Gerdes, R., Berger, W. (Eds.), *The Nordic Seas: An Integrated Perspective*. Geophys. Monogr. Ser., Vol. 158. American Geophys. Union, Washington, pp. 11-38.
- Boyer, T.P., Levitus, S., Antonov, J.I., Conkright, M. E., O'Brien, T., Stephens, C., 1998. *World Ocean Atlas 1998 Vol. 4: Salinity of the Atlantic Ocean*. NOAA Atlas NESDIS 30, U.S. Government Printing Office, Washington, D.C.
- Bromwich, D.H., Wang, S.H., 2005. Evaluation of the NCEP–NCAR and ECMWF 15- and 40-Yr Reanalyses Using Rawinsonde Data from Two Independent Arctic Field Experiments. *Mon. Wea. Rev.* 133, 3562–3578.

- Campin, J.-M., Marshall, J., Ferreira, D., 2008. Sea ice-ocean coupling using a rescaled vertical coordinate  $z^*$ , *Ocean Mod.*, 24(1-2), 1-14.
- Climatic Atlas of the Barents Sea: 1998, <http://www.nodc.noaa.gov/OC5/barsea/barindex1.html>.
- Cokelet, E. D., Tervalon, N., Bellingham, J. G., 2008. Hydrography of the West Spitsbergen Current, Svalbard Branch: Autumn 2001. *J. Geophys. Res.* 113, C01006, doi:10.1029/2007JC004150.
- Comiso, J., 1999. DMSP SSM/I daily polar gridded sea ice concentrations, June to September 2001. In: Maslanik, J., Stroeve, J., Boulder, CO: National Snow and Ice Data Center. Digital media, <http://nsidc.org/data/nsidc-0002.html>.
- Coward, A.C., De Cuevas, B.A., 2005. The OCCAM 66 level model: model description, physics, initial conditions and external forcing. Southampton Oceanography Centre Internal Document No.99, Southampton Oceanography Centre, 83pp.
- Dickson, R., Rudels, B., Dye, S., Karcher, M., Meincke, J., Yashayaev, I., 2007. Current estimates of freshwater flux through Arctic and subarctic seas. *Prog. Oceanogr.* 73(3-4), 210-230.
- Fahrbach, E., Østerhus, S., Schauer, U., Tverberg, V., Verduin, J., 2001. Direct measurements of volume transport through Fram Strait. *Polar Res.* 20(2), 217-224.
- Furevik, T., 2001. Annual and interannual variability of Atlantic Water temperatures in the Norwegian and Barents Seas: 1980-1996. *Deep-Sea Res. Part I* 48(2), 383-404.
- Furevik, T., Mauritzen, C., Ingvaldsen, R., 2007. The Flow of Atlantic Water to the Nordic Seas and Arctic Ocean. In: Ørbæk, J.B., Kallenborn, R., Tombre, I., Nøst Hegseth, E., Falk-Petersen, S., Hoel, A.H. (Eds.), *Arctic-Alpine Ecosystems and People in a Changing Environment*. Springer Verlag, Berlin, pp. 123-146.
- Gammelsrød, T., Leikvin, Ø., Lien, V., Budgell, W.P., Loeng, H., Maslowski, W., 2009. Mass and heat transports in the NE Barents Sea: Observations and models. *J. Mar. Sys.* 75, 56-69.
- Gascard, J.-C., Raisbeck, G., Sequeira, S., Yiou, F., Mork, K.A., 2004. The Norwegian Atlantic Current in the Lofoten basin inferred from hydrological and tracer data (129I) and its interaction with the Norwegian Coastal Current. *Geophys. Res. Lett.* 31, L01308.
- Gill, A.E., 1982. *Atmosphere-Ocean Dynamics*. New York: Academic Press, pp. 662.
- Gouretski, V.V., Jancke, K., 1996. A new hydrographic data set for the South Pacific: synthesis of WOCE and historical data. WHP SAC Technical Report 2, WOCE Report No 143/96, manuscript.
- Hansen, B., Østerhus, S., 2000. North Atlantic - Nordic Seas exchanges. *Prog. Oceanogr.* 45, 109-208.

- Hansen, B., Østerhus, S., Hátún, H., Kristiansen, R., Larsen, K.M.H., 2003. The Iceland-Faroe inflow of Atlantic water to the Nordic Seas. *Prog. Oceanogr.* 59, 443-474.
- Hanzlick, D., Aagaard, K., 1980. Freshwater and Atlantic Water in the Kara Sea. *J. Geophys. Res.* 85(C9), 4937-4942.
- Heil, P., Hibler, W.D., 2002. Modeling the High-Frequency Component of Arctic Sea Ice Drift and Deformation. *J. Phys. Oceanogr.* 32, 3039-3057.
- Holliday, N.P., Hughes, S.L., Bacon, S., Beszczynska-Möller, A., Hansen, B., Lavin, A., Loeng, H., Mork, K.A., Østerhus, S., Sherwin, T., Walczowski, W., 2008. Reversal of the 1960s to 1990s freshening trend in the northeast North Atlantic and Nordic Seas. *Geophys. Res. Lett.* 35, L03614.
- Holloway, G., Proshutinsky, A., 2007. Role of tides in Arctic ocean/ice climate. *J. Geophys. Res.* 112, C04S06.
- Hunke, E.C., 2001. Viscous plastic dynamics with the EVP model: Linearization issues. *J. Comput. Phys.* 170, 18-38.
- Ingvaldsen, R., Asplin, L., Loeng, H., 2004a. The seasonal cycle in the Atlantic transport to the Barents Sea during the years 1997-2001. *Cont. Shelf Res.* 24, 1015-1032.
- Ingvaldsen, R.B., Asplin, L., Loeng, H., 2004b. Velocity field of the western entrance to the Barents Sea. *J. Geophys. Res.* 109, C03021.
- Ivanov, V.V., Golovin, P.N., 2007. Observations and modeling of dense water cascading from the northwestern Laptev Sea shelf. *J. Geophys. Res.* 112, C09003, doi: 10.1029/2006JC003882.
- Ivanov, V.V., Shapiro, G.I., 2005. Formation of a dense water cascade in the marginal ice zone in the Barents Sea. *Deep-Sea Res. Part I* 52, 1699-1717.
- Ivanov, V.V., Shapiro, G.I., Huthnance, J.M., Aleynik D.L., Golovin, P.N., 2004. Cascades of dense water around the world ocean. *Prog. Oceanogr.* 60(1), 47-98.
- Jakobsen, P.K., Ribergaard, M.H., Quadfasel, D., Schmith, T., Hughes, C. W., 2003. Near-surface circulation in the northern North Atlantic as inferred from Lagrangian drifters: Variability from the mesoscale to interannual. *J. Geophys. Res.* 108(C8), 3251.
- Jakobsson, M., Cherkis, N., Woodward, J., Macnab, R. Coakley, B., 2000. New grid of Arctic bathymetry aids scientists and mapmakers, *Eos Trans. AGU*, 81, 89, 93, 96.
- Jerlov, N. G., 1968. *Optical Oceanography*. Elsevier, 194 pp.
- Karcher, M. J., Oberhuber, J. M., 2002. Pathways and modification of the upper and intermediate

- waters of the Arctic Ocean. *J. Geophys. Res.* 107(C6), 3049, doi:10.1029/2000JC000530.
- Kay, J. E., L'Ecuyer, T., Gettelman, A., Stephens, G., O'Dell, C., 2008. The contribution of cloud and radiation anomalies to the 2007 Arctic sea ice extent minimum. *Geophys. Res. Lett.* 35, L08503.
- Killworth, P.D., Stainforth, D., Webb, D.J., Paterson, S.M., 1991. The development of a free-surface Bryan-Cox-Semtner ocean model. *J. Phys. Oceanogr.* 21(9), 1333-1348.
- Kwok, R., Cunningham, G.F., Pang, S.S., 2004. Fram Strait sea ice outflow. *J. Geophys. Res.* 109(C1), C01009.
- Large, W.G., McWilliams, J.C., Doney S.C., 1994. Oceanic Vertical Mixing: A Review and a Model with a Nonlocal Boundary-Layer Parameterization. *Rev. Geophys.* 32(4), 363-403.
- Large, W.G., Danabasoglu, G., Doney, S.C., 1997. Sensitivity to surface forcing and boundary layer mixing in a global ocean model: annual-mean climatology. *J. Phys. Oceanogr.* 27, 2418-2446.
- Leppäranta, M., Omstedt, A., 1990. Dynamic coupling of sea ice and water for an ice field with free boundaries, *Tellus*, 42A(4), 482-495.
- Lindsay, R.W., Zhang, J., 2005. The thinning of Arctic Sea Ice, 1988–2003: have we passed a tipping point? *J. Clim.* 18(22), 4879-4894.
- Loeng, H., 1991. Features of the physical oceanographic conditions of the Barents Sea. *Polar Res.* 10(1), 5-18.
- Loeng, H., Ozhigin, V., Ådlandsvik, B., 1997. Water fluxes through the Barents Sea. *ICES J. Mar. Sci.* 54, 310–317.
- Marshall, J., Schott, F., 1999. Open-Ocean Convection: Observations, Theory, and Models, *Rev. Geophys.*, 37(1), 1–64.
- Maslowski, W., Marble, D., Walczowski, W., Schauer, U., Clement, J.L., Semtner, A.J., 2004. On climatological mass, heat, and salt transports through the Barents Sea and Fram Strait from a pan-Arctic coupled ice-ocean model simulation. *J. Geophys. Res.* 109, C03032.
- Mauritzen, C., 1996. Production of dense overflow waters feeding the North Atlantic across the Greenland-Scotland Ridge. Part 1: Evidence for a revised circulation scheme. *Deep-Sea Res. Part I* 43(6), 769-806.
- McClimans, T.A., Johnson, D.A., Krosshavn, M., King, S.E., Carroll, J.-L., Grenness, Ø., 2000. Transport processes in the Kara Sea. *J. Geophys. Res.* 105(C6), 14,121–14,139.

- McPhee, M.G., 1984. Drift velocity during the drift-station phase of MIZEX 83, *MIZEX Bull. IV*, 1-11, US CRREL, Hanover, N.H.
- Middtun, L., 1985. Formation of dense bottom water in the Barents Sea. *Deep-Sea Res. A* 32, 1233-41.
- Oliver, K.I.C., Heywood, K.J., 2003. Heat and Fresh Water Fluxes through the Nordic Seas. *J. Phys. Oceanogr.* 33, 1009-1026.
- Olsen, S.M., Schmith, T., 2007. North Atlantic – Arctic Mediterranean exchanges in an ensemble hindcast experiment. *J. Geophys. Res.* 112, C04010, doi:10.1029/2006JC003838.
- Orvik, K.A., 2004. The deepening of the Atlantic water in the Lofoten Basin of the Norwegian Sea, demonstrated by using an active reduced gravity model. *Geophys. Res. Lett.* 31, L01306.
- Orvik, K.A., Mork, M., 1996. Atlantic water transport from long term current measurements in the Svinøy section. *ICES C.M. Documents* 1996/O:8, 1-9.
- Orvik, K.A., Niiler, P., 2002. Major pathways of Atlantic water in the northern North Atlantic and Nordic Seas toward Arctic. *Geophys. Res. Lett.* 29(19), 1896.
- Orvik, K.A., Skagseth, Ø., 2005. Heat flux variations in the eastern Norwegian Atlantic Current toward the Arctic from moored instruments, 1995-2005. *Geophys. Res. Lett.* 32, L14610.
- Orvik, K.A., Skagseth, Ø., Mork, M., 2001. Atlantic inflow to the Nordic Seas: current structure and volume fluxes from moored current meters, VM-ADCP and SeaSoar-CTD observations 1995-1999. *Deep-Sea Res. Part I* 48, 937-957.
- Østerhus, S., Turrell, W.R., Jónsson, S., Hansen, B., 2005. Measured volume, heat, and salt fluxes from the Atlantic to the Arctic Mediterranean. *Geophys. Res. Lett.* 32, L07603.
- Ozhigin, V.K., Trofimov, A.G., Ivshin, V.A., 2000. The Eastern Basin Water and currents in the Barents Sea. *ICES* 2000/L:14, 1-19.
- Pacanowski, R.C., Gnanadesikan, A., 1998. Transient Response in a Z-Level Ocean Model That Resolves Topography with Partial Cells. *Mon. Weather Rev.* 126(12), 3248–3270.
- Pantelev, G.G., Ikeda, M., Grotov, A., Nechaev, D.A., Yaremchuk, M., 2004. Mass, heat and salt balances in the Eastern Barents Sea obtained by inversion of hydrographic section data. *J. Oceanogr., The Oceanographic Society of Japan* 60, 613-623.
- Pantelev, G., Proshutinsky, A., Kulakov, M., Nechaev, D.A., Maslowski, W., 2007. Investigation of the summer Kara Sea circulation employing a variational data assimilation technique. *J. Geophys. Res.* 112, C04S15.

- Paulson, C.A., Simpson, J.J., 1977. Irradiance measurements in the upper ocean. *J. Phys. Oceanogr.* 7, 952-956.
- Pfirman, S.L., Bauch, D., Gammelsrød, T., 1994. The North Barents Sea: Water mass distribution and modification. In: Johannessen, O.M., Muench, R.D., Overland, J.E. (Eds.), *The Polar Oceans and their Role in Shaping the Global Environment. Geophys. Monogr. Ser., Vol. 85.* American Geophys. Union, Washington, pp. 77-94.
- Piechura, J., Beszczynska-Moeller, A., Osinski, R., 2001. Volume, heat and salt transport by the west spistbergen current. *Polar Res.* 20(2), 233-240.
- Polyakov, I.V., Beszczynska, A., Carmack, E.C., Dmitrenko, I. A., Fahrbach, E., Frolov, I.E., Gerdes, R., Hansen, E., Holfort, J., Ivanov, V.V., Johnson, M.A. Karcher, M., Kauker, F., Morison, J., Orvik, K.A., Schauer, U., Simmons, H.L., Skagseth, Ø., Sokolov, V.T., Steele, M., Timokhov, L.A., Walsh, D., Walsh, J.E., 2005. One more step toward a warmer Arctic. *Geophys. Res. Lett.* 32, L17605.
- Polyakov, I.V., Johnson, M.A., 2000. Arctic decadal and interdecadal variability. *Geophys. Res. Lett.* 27(24), 4097-4100.
- Poulain, P.-M., Warn-Varnas, A., Niiler, P.P., 1996. Near-surface circulation of the Nordic seas as measured by Lagrangian drifters. *J. Geophys. Res.* 101(C8), 18237-18258.
- Proshutinsky, A., Kowalik, Z., 2007. Preface to special section on Arctic Ocean Model Intercomparison Project (AOMIP) Studies and Results. *J. Geophys. Res.* 112, C04S01, doi:10.1029/2006JC004017.
- Quadfasel, D., Rudels, B., Selchow, S., 1992. The Central Bank vortex in the Barents Sea: watermass transformation and circulation. *ICES Mar. Sci. Symp.* 195, 40-51.
- Romanov, I.P., 1995. *Atlas of Ice and Snow of the Arctic Basin and Siberian Shelf Seas.* A. Tunik (Ed.), Backbone Publishing Company. 277 pp.
- Rosby, T., Ozhigin, V., Ivshin, V., Bacon, S., 2007. An isopycnal analysis of the Nordic Seas hydrography. International Council for the Exploration of the Sea, Contribution to Statutory Meeting, Oceanography Committee, Annex 5, ICES C.M.2007/OCC:05, 12-31.
- Rossov, W.B., Schiffer, R.A., 1991. ISCCP Cloud Data Products. *Bulletin of the American Meteorological Society* 72, 2-20.

- Rudels, B., Björk, G., Nilsson, J., Winsor, P., Lake I., Nohr, C., 2005. The interaction between waters from the Arctic Ocean and the Nordic Seas north of Fram Strait and along the East Greenland Current: results from the Arctic Ocean-02 Oden expedition. *J. Mar. Syst.* 55(1-2), 1-30.
- Rudels, B., Friedrich, H.J., 2000. Transformations of the Atlantic Water in the Arctic Ocean and their significance for the freshwater budget. In: Lewis, E.L. et al. (Eds.), *The Freshwater Budget of the Arctic Ocean*. Kluwer, The Netherlands, pp. 503-532.
- Sætre, R., 1999. Features of the central Norwegian shelf circulation. *Cont. Shelf Res.* 19(14), 1809-1831.
- Saloranta, T.M., Haugan, P.M., 2001. Interannual variability in the hydrography of Atlantic water northwest of Svalbard. *J. Geophys. Res.* 106(C7), 13931-13943, 2000JC000487.
- Sandwell, D.T., Smith, W.H.F., 1995. *Marine Gravity from satellite Altimetry*. The Geological Data Center, Scripps Institution of Oceanography, digital file V7.2.
- Schauer, U., 1995. The release of brine-enriched shelf water from Storfjord into the Norwegian Sea. *J. Geophys. Res.* 100(C8), 16015-16028.
- Schauer, U., Fahrbach E., 1999. A dense bottom water plum in the western Barents Sea: downstream modification and interannual variability. *Deep-Sea Res. Part I* 46, 2095-2108.
- Schauer, U., Loeng, H., Rudels, B., Ozhigin, V.K., Dieck, W., 2002. Atlantic Water flow through the Barents and Kara Seas. *Deep-Sea Res. Part I* 49, 2281-2298.
- Schauer, U., Muench, R.D., Rudels, B., Timokhov, L., 1997. Impact of eastern Arctic shelf waters on the Nansen Basin intermediate layers. *J. Geophys. Res.* 102(C2), 3371-3382.
- Schauer, U., Østerhus, S., Rohardt, G., 2004. Arctic Warming through the Fram Strait: Oceanic heat transport from 3 years of measurement. *J. Geophys. Res.* 109, C06026.
- Semtner, A.J., 1976. A model for the thermodynamic growth of sea ice in numerical investigation of climate. *J. Phys. Oceanogr.* 6, 376-389.
- Simonsen, K., Haugan, P., 1996. Heat budgets of the Arctic Mediterranean and sea surface heat flux parameterizations for the Nordic Seas. *J. Geophys. Res.* 101, 6553-6576.
- Skagseth, Ø., Furevik, T., Ingvaldsen, R., Loeng, H., Mork, K.A., Orvik, K.A., Ozhigin, V., 2008. Volume and heat transports to the Arctic Ocean via the Norwegian and Barents Seas. *Arctic-Subarctic Ocean Fluxes: Defining the Role of the Northern Seas in Climate*; Dickson, R.R., Meincke, J., Rhines, P. (Eds.). Springer Verlag, Netherlands, 45-64.

- Slagstad, D., McClimans, T.S., 2005. Modeling the ecosystem dynamics of the Barents Sea including the marginal ice zone: I. Physical and chemical oceanography. *J. Mar. Syst.* 58(1-2), 1-18.
- Speer, K.G., 1993. Conversion among North-Atlantic surface-water types. *Tellus, A.* 45A, 72-79.
- Spencer, R.W., 1993. Global oceanic precipitation from MSU during 1979-91 and comparisons to other climatologies. *J. Clim.* 6, 1301-1326.
- Steele, M., Boyd, T., 1998. Retreat of the cold halocline layer in the Arctic Ocean. *J. Geophys. Res.* 103(C5), 10419-10435.
- Steele, M., Morison, J., Curtin, T., 1995. Halocline water formation in the Barents Sea. *J. Geophys. Res.* 100(C1), 881-894.
- Steele, M., Morley, R., Ermold, W., 2001. PHC: A global ocean hydrography with a high quality Arctic Ocean. *J. Clim.* 14(9), 2079-2087.
- Stroeve, J.C., Serreze, M.C., Fetterer, F., Arbetter, T., Meier, W., Maslanik, J., Knowles, K., 2005. Tracking the Arctic's shrinking ice cover: Another extreme September minimum in 2004. *Geophys. Res. Lett.* 32, L04501.
- Stouffer, R.J., Yin, J., Gregory, J.M., Dixon, K.W., Spelman, M.J., Hurlin, W., Weaver, A.J., Eby, M., Flato, G.M., Hasumi, H., Hu, A., Jungclaus, J.H., Kamenkovich, I.V., Levermann, A., Montoya, M., Murakami, S., Nawrath, S., Oka, A., Peltier, W.R., Robitaille, D.Y., Sokolov, A., Vettoretti, G., Weber, S. L., 2006. Investigating the Causes of the Response of the Thermohaline Circulation to Past and Future Climate Changes. *J. Clim.* 19(8), 1365-1387.
- Vellinga, M., Wood, R.A., 2002. Global climate impacts of a collapse of the Atlantic thermohaline circulation. *Clim. Change* 54, 251-267.
- Vinje, T., Kvambekk, A.S., 1991. Barents Sea drift ice characteristics. *Polar Res.* 10(1), 59-68.
- Walczowski, W., Piechura, J., 2007. Pathways of the Greenland Sea warming. *Geophys. Res. Lett.* 34, L10608.
- Webb, D.J., de Cuevas, B.A., Richmond, C.S., 1998. Improved advection schemes for ocean models. *J. Atmos. Oceanic Technol.* 15(5), 1171-1187.
- World Ocean Atlas 2005, [http://www.nodc.noaa.gov/OC5/WOA05/pr\\_woa05.html](http://www.nodc.noaa.gov/OC5/WOA05/pr_woa05.html).
- Wu, P., Haak, H., Wood, R., Jungclaus, J., Furevik, T. 2008. Simulating the terms in the Arctic hydrological budget. *Arctic-Subarctic Ocean Fluxes: Defining the Role of the Northern Seas in Climate*; Dickson, R.R., Meincke, J., Rhines, P. (Eds.). Springer Verlag, Netherlands, 363-384.

Table 1. Simulated and observed volume, quasi-heat and total salinity transports associated with the NAW core ( $S \geq 35.00$ ,  $T \geq 2.0^\circ\text{C}$ ) in the Nordic Seas. Maximum depth of the core is shown. The quasi-heat transport is referenced to  $-0.1^\circ\text{C}$ . All transports are positive northwards. Observations are shown in bold. N/A – not available from the literature. Section numbers are in brackets and their positions are shown in Figure 3b. ( $1 \text{ Sv} = 10^6 \text{ m}^3 \cdot \text{s}^{-1}$ ;  $1 \text{ TW} = 10^{12} \text{ W}$ ;  $1 \text{ kT} = 10^6 \text{ kg} \cdot \text{s}^{-1}$ ).

Hydro-graphic section	Ocean Volume Transport [Sv]	Ocean Salt Transport [ $\text{kT} \cdot \text{s}^{-1}$ ]	Ocean Quasi-Heat Transport [TW]	Mean Temp. [ $^\circ\text{C}$ ]	Mean Salinity	Maximum core depth [m]
Svinøy (4)	5.6±0.8	200±28	160±23	5.9±0.7 8.0±0.7*	35.18±0.04	546
	<b>5.3<sup>a</sup>-7.6<sup>b</sup></b>	N/A	<b>133±11<sup>e</sup></b>	<b>8.1±0.6<sup>f*</sup></b>	<b>35.23±0.05<sup>g</sup></b>	<b>500</b>
Gimsøy (5)	6.5±1.4	236±50	148±32	4.2±0.5 5.7±0.5*	35.08±0.02 35.06±0.03*	678
	<b>7.2<sup>c</sup></b>	N/A	N/A	<b>6.7±0.5<sup>f*</sup></b>	<b>35.14±0.04<sup>f*</sup></b>	<b>640-750</b>
Bjørnøya West (6)	5.7±1.3 2.3±0.7*	206±46	111±25	4.3±0.3	35.08±0.01	678
	<b>2.1<sup>d*</sup></b>	N/A	N/A	N/A	N/A	N/A
Sørkapp (7)	4.4±1.4	160±49	80±25	3.7±0.3	35.06±0.01	609
	N/A	N/A	N/A	<b>3.9±0.7<sup>f</sup></b>	<b>35.07±0.04<sup>g</sup></b>	<b>600</b>

Key: <sup>a</sup> – Orvik and Mork, 1996; <sup>b</sup> – Orvik et al., 2001; <sup>c</sup> – Gascard et al., 2004; <sup>d</sup> – Piechura et al., 2001; <sup>e</sup> – Orvik and Skagseth, 2005; <sup>f</sup> – Blindheim and Østerhus, 2005; <sup>g</sup> – Skagseth et al., 2008; \* calculations for the layer 50-200 m for summer months (July-Aug-Sept).

Table 2. Mean cross-section velocity, heat and total salinity transports associated with NAW inflow across Greenland-Scotland Ridge from model and observations. Model data are averaged for the period 1989-2004. In Denmark Strait NAW for the top 200 m is considered; for the other two sections NAW is with  $T \geq 5.0^\circ\text{C}$  and  $S \geq 35.00$ . Enthalpy transport is taken for a proxy of the heat transport and is referenced to  $0^\circ\text{C}$ . All transports are positive northwards. Observed values from Østerhus et al. (2005) are shown in bold. Section numbers are in brackets and their positions are shown in Figure 3a.  $1 \text{ Sv} = 10^6 \text{ m}^3 \cdot \text{s}^{-1}$ ;  $1 \text{ TW} = 10^{12} \text{ W}$ ;  $1 \text{ kT} = 10^6 \text{ kg} \cdot \text{s}^{-1}$ .

Hydrographic section	Denmark Strait (1)	Iceland-Faroe (2)	Faroe-Shetland (3)
Ocean volume transport [Sv]	1.0±0.4 <b>0.8±0.5</b>	3.1±0.5 <b>3.8±0.5</b>	3.4±0.8 <b>3.8±0.5</b>
Ocean Heat Transport [TW]	13.0±7.0 <b>22</b>	104.3±17.3 <b>134</b>	135.6±29.9 <b>156</b>
Ocean Salt Transport [kT·s <sup>-1</sup> ]	36.0±13.0 <b>30</b>	110.7±19.0 <b>133</b>	123.0±29.6 <b>139</b>
Mean Ocean Temperature [°C]	6.2±0.5 <b>6.0</b>	8.1±0.5 <b>8.2</b>	8.5±0.7 <b>9.5</b>
Mean Salinity	35.20±0.04 <b>35.00</b>	35.34±0.05 <b>35.23</b>	35.36±0.03 <b>35.32</b>

Table 3. As Table 2, but for the simulated NAW (with  $S \geq 34.80$ ,  $T \geq 1.0^\circ\text{C}$ ) transports in Fram Strait and the Barents Sea. Heat transport is referenced to  $-0.1^\circ\text{C}$ .

Hydrographic section	Ocean Volume Transport [Sv]	Ocean Salt Transport [kT·s <sup>-1</sup> ]	Ocean Heat Transport [TW]	Mean Ocean Temperature [°C]	Mean Salinity
Norway–Bjørnøya (8)	1.7±0.5	60.4±19.2	44.4±10.1	5.2±0.4	35.01±0.03
Bjørnøya–Svalbard (9)	0.01±0.02	0.5±0.7	0.2±0.3	2.1±0.6	34.85±0.05
KB (10)	1.0±1.2	37.4±42.7	17.0±18.3	2.7±0.6	35.03±0.02
WSC (10)	2.1±1.2	73.9±44.0	27.7±14.7	3.2±0.6	35.03±0.02
YPB (11)	1.9±1.2	67.3±41.9	25.4±14.4	3.1±0.6	35.03±0.03
SVB (11)	0.4±0.2	13.5±7.0	4.9±2.4	3.3±0.7	35.02±0.04

Table 4. As Table 3, but for the total net transports.

Hydrographic section	Ocean Volume Transport [Sv]	Ocean Salt Transport [ $\text{kT}\cdot\text{s}^{-1}$ ]	Ocean Heat Transport [TW]	Mean Ocean Temperature [ $^{\circ}\text{C}$ ]	Mean Salinity
Norway–Bjørnøya (8)	2.2±0.8	80.3±28.0	59.9±17.9	4.8±0.5	34.96±0.04
Bjørnøya–Svalbard (9)	-0.1±0.1	-1.8±3.8	0.6±0.6	-0.4±0.9	34.44±0.13
KB (10)	1.2±1.5	44.5±55.3	16.6±18.4	0.6±0.2	34.94±0.01
WSC (10)	2.2±1.3	79.8±48.3	28.4±15.1	2.5±0.5	34.99±0.02
YPB (11)	2.0±1.3	71.1±45.1	26.0±14.7	2.4±0.5	34.89±0.05
SVB (11)	0.4±0.2	15.1±8.6	5.1±2.5	2.9±0.7	35.00±0.02
Svalbard–Franz-Josef Land (12)	0.4±0.2	14.1±7.1	-0.5±0.7	0.2±0.3	34.41±0.06

Table 5. As Table 4, but for the Kara Sea.

Hydrographic section	Ocean Volume Transport [Sv]	Ocean Salt Transport [ $\text{kT}\cdot\text{s}^{-1}$ ]	Ocean Heat Transport [TW]	Mean Ocean Temperature [ $^{\circ}\text{C}$ ]	Mean Salinity
Franz-Josef Land–Novaya Zemlya (13)	1.4±0.6	50.2±19.4	-4.0±2.2	-0.9±0.1	34.44±0.05
Kara Gate (14)	0.3±0.2	9.9±6.2	-1.4±1.2	-1.3±0.6	33.47±0.34
St. Anna Trough (15)	1.4±0.5	50.4±17.9	-5.0±1.8	0.5±0.3	34.54±0.04
Voronin Trough (16)	0.2±0.1	6.3±3.1	-1.32±0.6	-1.3±0.1	33.80±0.09
Wilkitsky Strait (17)	0.1±0.1	3.6±4.4	-0.8±0.8	-1.5±0.1	32.50±0.24
Shokalsky Strait (18)	0.02±0.01	0.7±0.3	-0.2±0.1	-1.5±0.1	32.77±0.14

Table 6. Averaged for the period 1989-2004 simulated water mass transformation rates of the halocline waters CHW-CDW (with  $S < 34.80$ ,  $T < 0^{\circ}\text{C}$ ) and NAW (with  $S \geq 34.80$ ,  $T \geq 1.0^{\circ}\text{C}$ ) in the Barents Sea. Positive rates indicate the watermass gain. For the areas see Figure 12.

	Area (IV)	Area (III)	Area (IIIa)
Transformation rate due to the atmospheric forcing [Sv] NAW	0.257	0.079	0.021
Transformation rate due to the atmospheric forcing [Sv] CHW-CDW	1.531	0.740	0.169
Transformation rate due to the atmospheric forcing [Sv] NAW	-1.012	-1.051	-0.113
Transformation rate due to the atmospheric forcing [Sv] CHW-CDW	-0.614	-0.033	0.042

**List of captions**

Figure 1. Global mean (per unit volume) oceanic kinetic energy (KE) of the ocean in the 1/12° model.

Figure 2. Bathymetry (IBCAO 2-km dataset) of: (a) - the Nordic Seas; (b) - the Eurasian Arctic. For abbreviations see Appendix.

Figure 3. Simulated mean ocean velocities in  $\text{m s}^{-1}$  (sticks) and potential temperature in  $^{\circ}\text{C}$  (colour-coded) averaged for the period 1989-2004 in the 1/12° model at the depth of 166 m in (a) - the Nordic Seas; (b) – the same for the Eurasian Arctic at the depth of 120 m. Currents associated with the NAW inflow are indicated. One out of sixteen velocity nodes per area is shown. Hydrographic sections are shown as blue lines (numbers 1-18). For abbreviations see Appendix.

Figure 4. (a) - Salinity for the specific volume anomaly surface  $\Delta = 2.1\text{e-}7 \text{ m}^3 \text{ kg}^{-1}$  for April-June 1951–2000 from hydrographic stations; (b) - Simulated salinity on the density surface  $\sigma_2 = 37.174$  averaged for April–June 1989-2004 in the 1/12° model.

Figure 5. Simulated flow through the eastern Fram Strait (hydrographic section 10) averaged for the period 1989-2004 in the 1/12° model: (a) - mean-annual cross-section ocean velocities in  $\text{cm s}^{-1}$  (solid contours–northward flow, dashed contours–southward flow) and salinity (colour-coded); (b) – mean-annual potential temperature in  $^{\circ}\text{C}$  (colour-coded). Selected currents and water masses are marked. For abbreviations see Appendix.

Figure 6. As Figure 5, but for the passage Svalbard-Franz-Josef Land (hydrographic section 12).

Figure 7. Simulated flow of NAW between Franz-Josef Land and Novaya Zemlya (hydrographic section 13) averaged for the period 1989-2004 in the 1/12° model: (a) - mean-annual cross-section ocean velocities in  $\text{cm s}^{-1}$  (solid contours–eastward flow, dashed contours–westward flow) and potential temperature in  $^{\circ}\text{C}$  (colour-coded); (b) – mean-annual salinity (colour-coded). Selected currents and water masses are marked. For abbreviations see Appendix.

Figure 8. As Figure 5, but for the St. Anna Trough and Voronin Trough (hydrographic sections 15, 16).

Figure 9. As Figure 5, but for the western Barents Sea (hydrographic sections 8 and 9). Solid contours show eastward flow, dashed contours–westward flow.

Figure 10. Simulated maximum mixed layer depth in [m] (colour-coded) averaged for the period 1989-2004 in the  $1/12^\circ$  model and mixed layer depth derived from World Ocean Atlas Climatology (contours). Dashed lines show simulated September (red) and March (blue) ice extent averaged for the period 1989-2004. Stars and small letters with numbers indicate convection sites in Central Basin (c1-c5), around Franz-Josef Land (f1-f2), west and northwest of Novaya Zemlya (n1-n4) and in the vicinity of Svalbard (s1-s3); cyan stars mark full-depth and yellow ones - shallow convection sites.

Figure 11. Simulated maximum mixed layer depth in [m] (colour-coded) in March (a) 1989, (b) 1995, (c) 2001; ice edge in March (blue) and August (red) is shown; (d) time evolution of the maximum mixed layer depth at the convection sites together with ice production (for details see Section 4) in the Barents Sea. Upper panel in (d) depicts maximum mixed layer depth at deep convective sites c1-c4 (blue, red, green, cyan), f1 (magenta), n1 (yellow) and s1 (black). Middle panel in (d) shows maximum mixed layer depth at St. Anna Trough convective site n4 (black) and ice production averaged for the area of convection site (red). Lower panel in (d) shows maximum mixed layer depth at intermediate-depth convective sites c5 (blue), f2 (red) and s3 (green).  $1/12^\circ$  model results.

Figure 12. Schematic of the North Atlantic Inflow into the Arctic Ocean from the  $1/12^\circ$  model drawn over the model bathymetry. Red arrows show the warm FSB; light-blue - pathway of the cold and fresh CHW and CDW within the FJB; cyan - pathways of the BBW within the NZB; roman numerals indicate regions with different NAW inflow regimes. Stars are as in Figure 10 with black arrows showing pathways of sinking water.

Figure 1

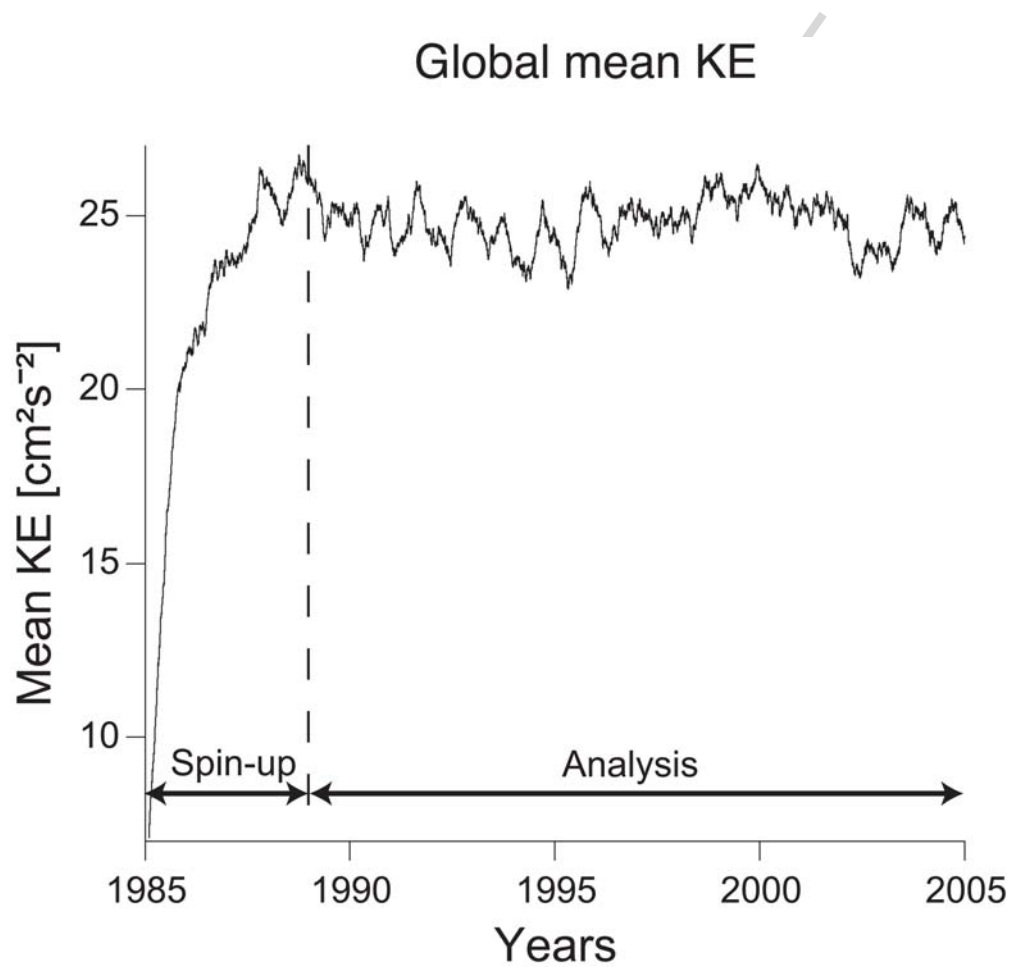


Figure 2a

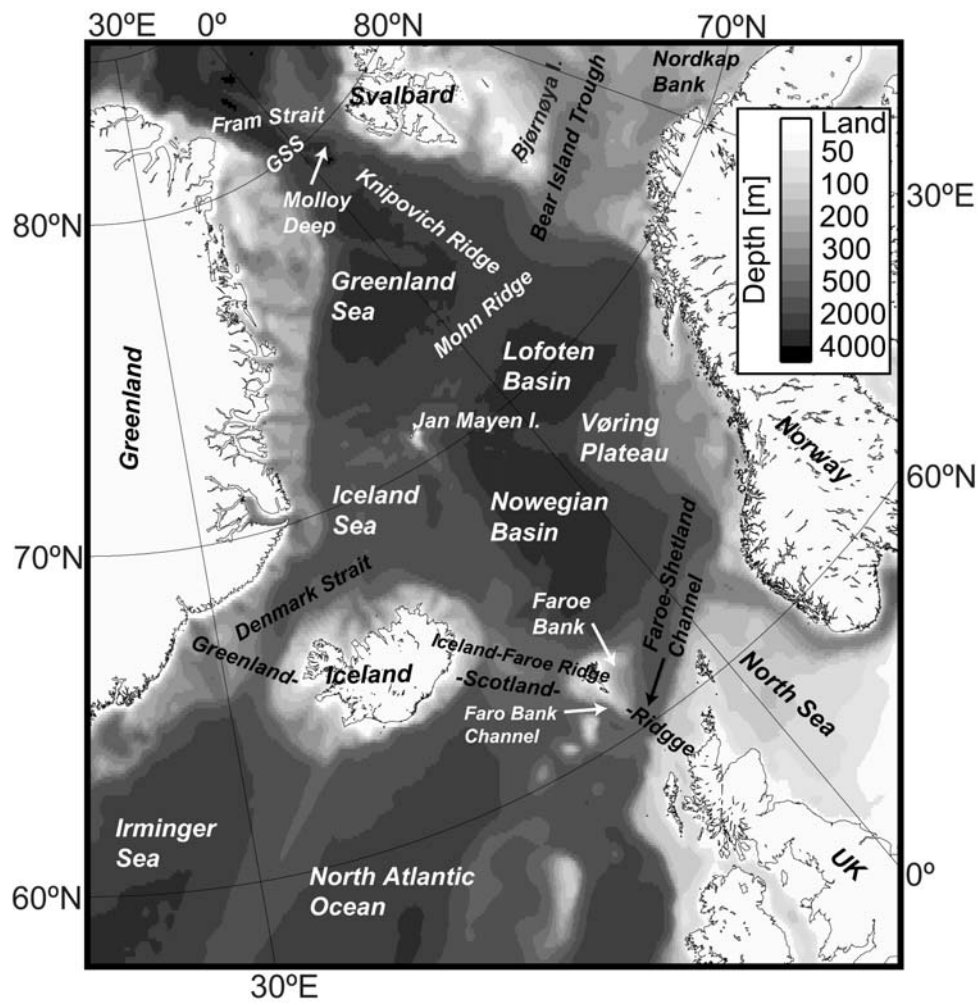


Figure 2b

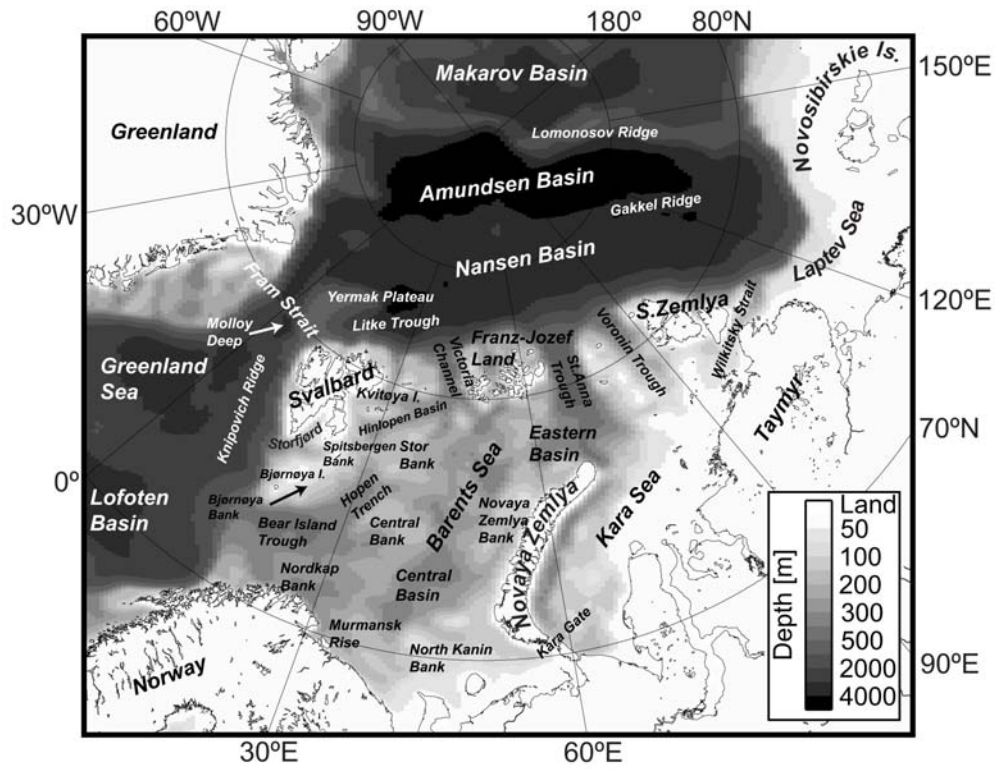


Figure 3a

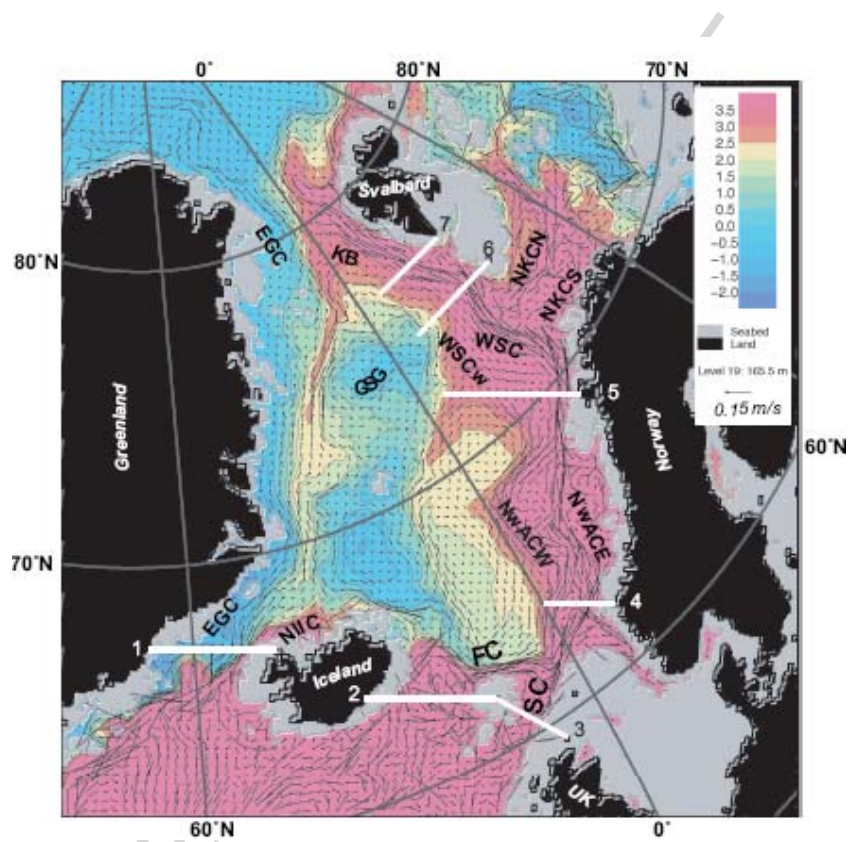


Figure 3b

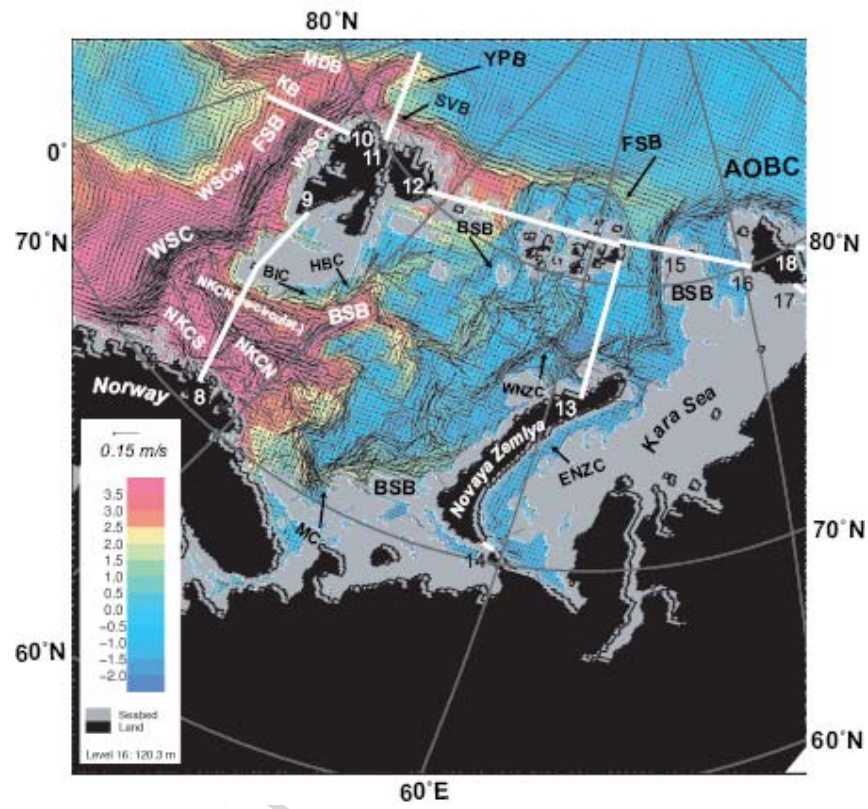


Figure 4a

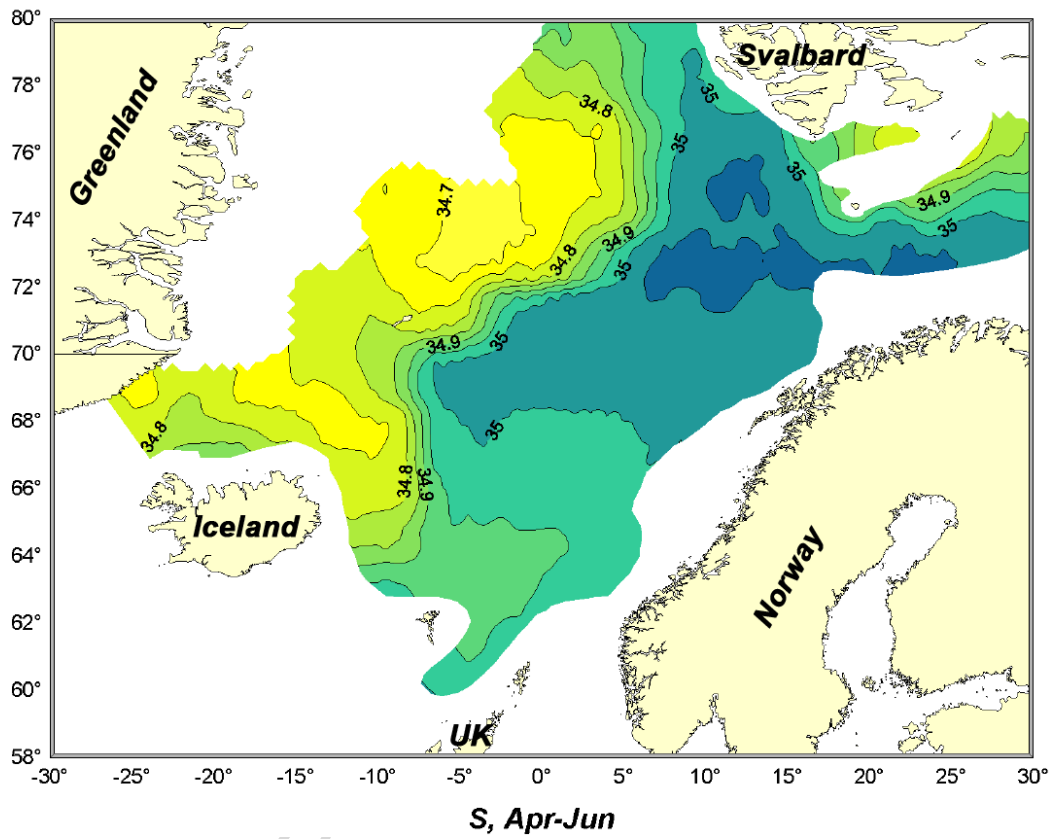


Figure 4b

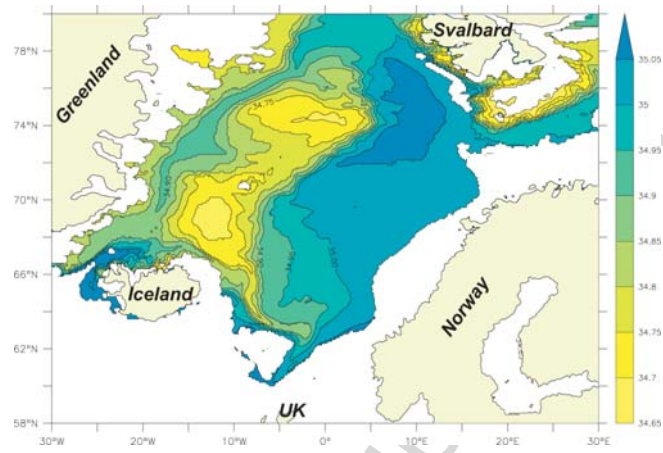


Figure 5a

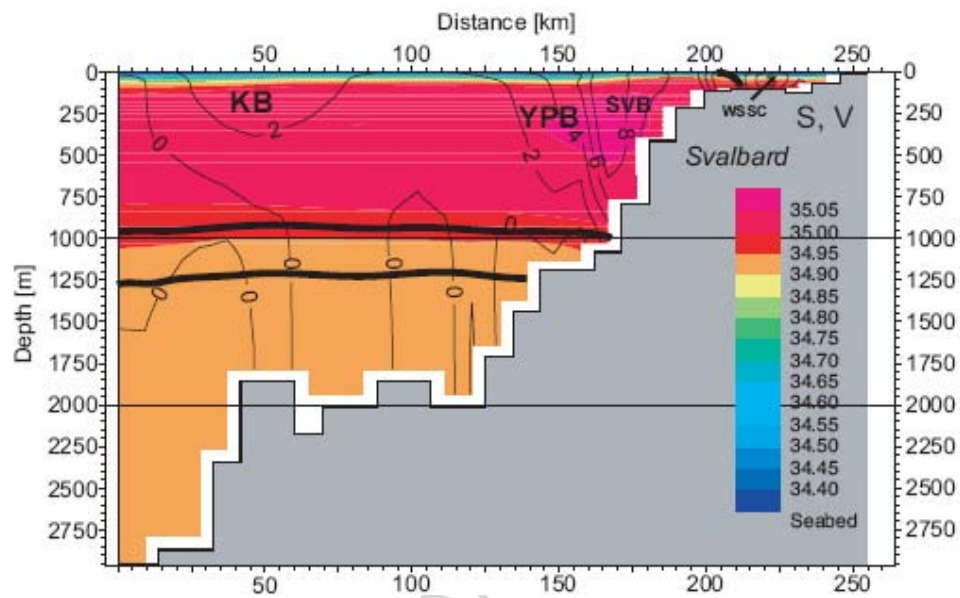


Figure 5b

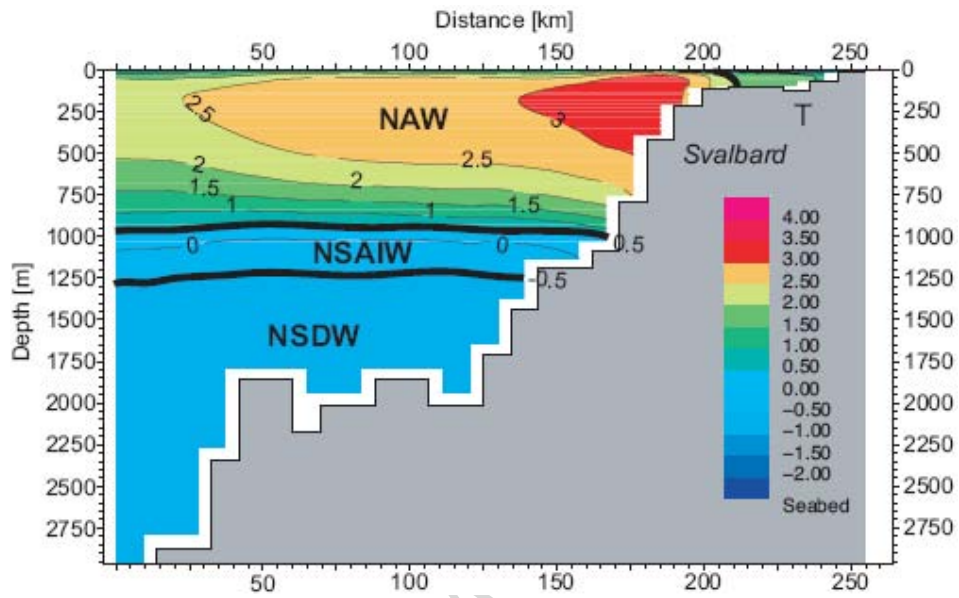


Figure 6a

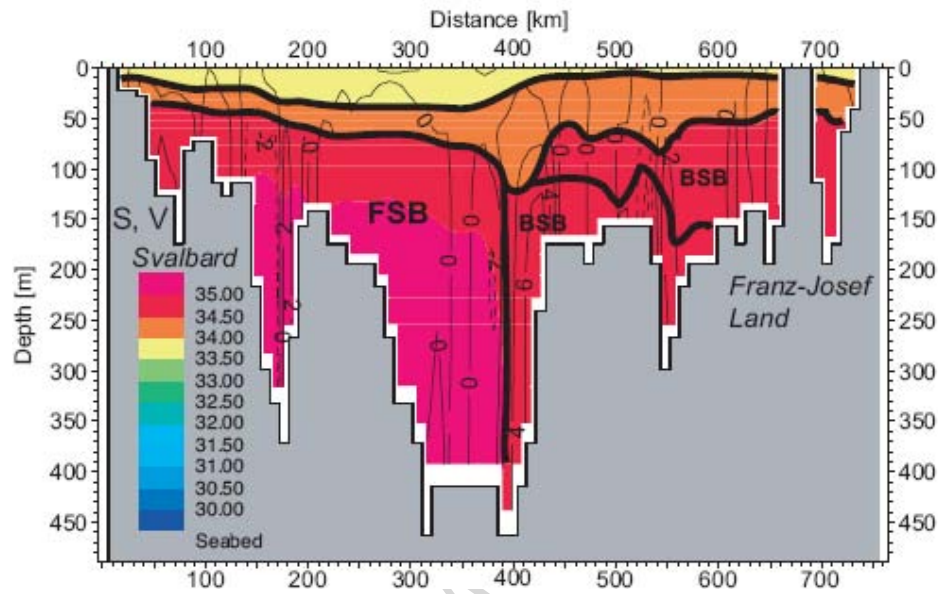


Figure 6b

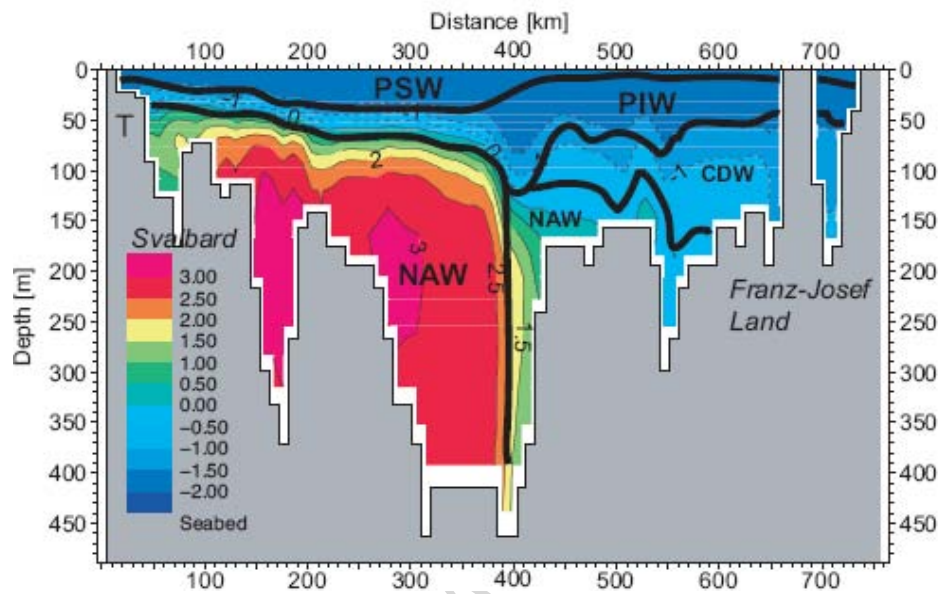


Figure 7a

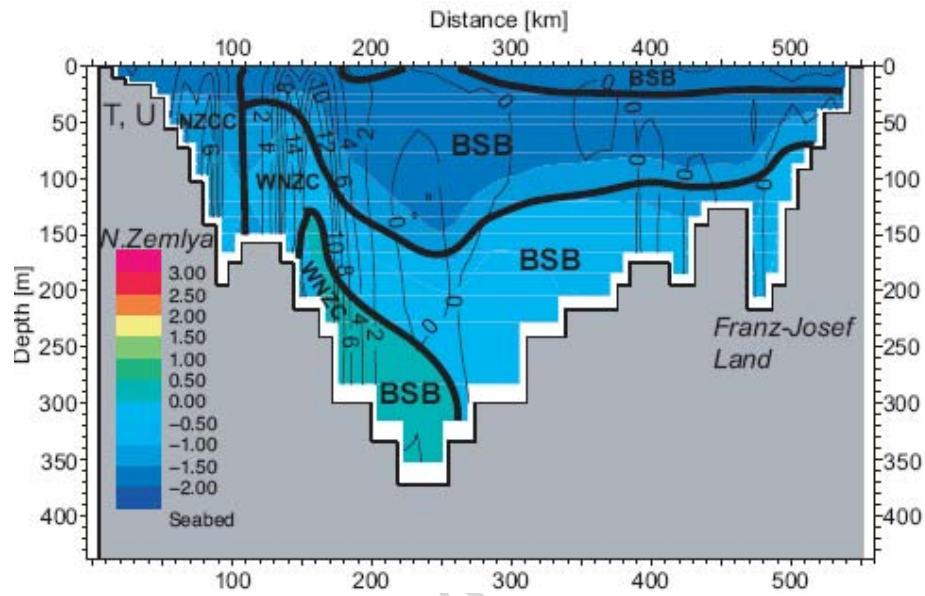


Figure 7b

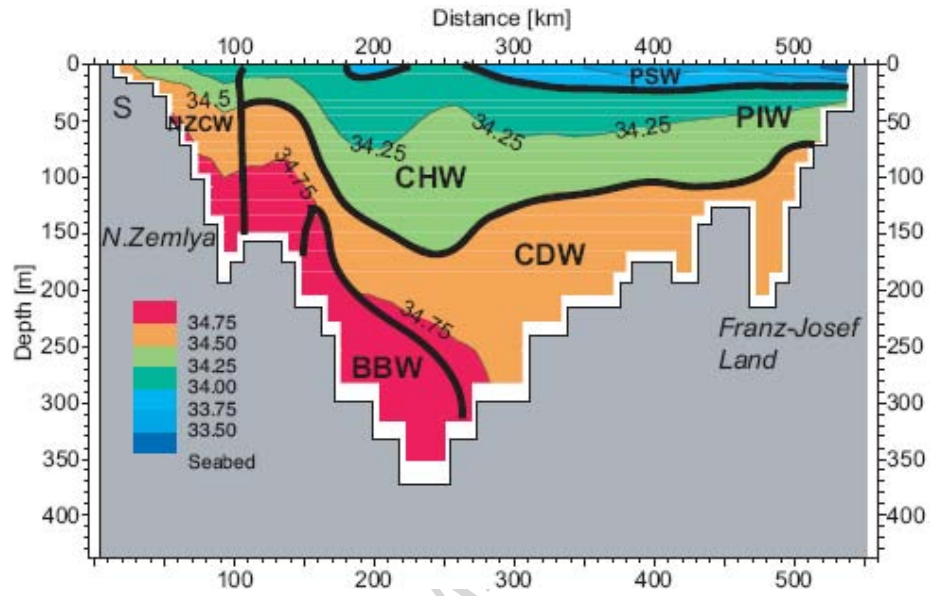


Figure 8a

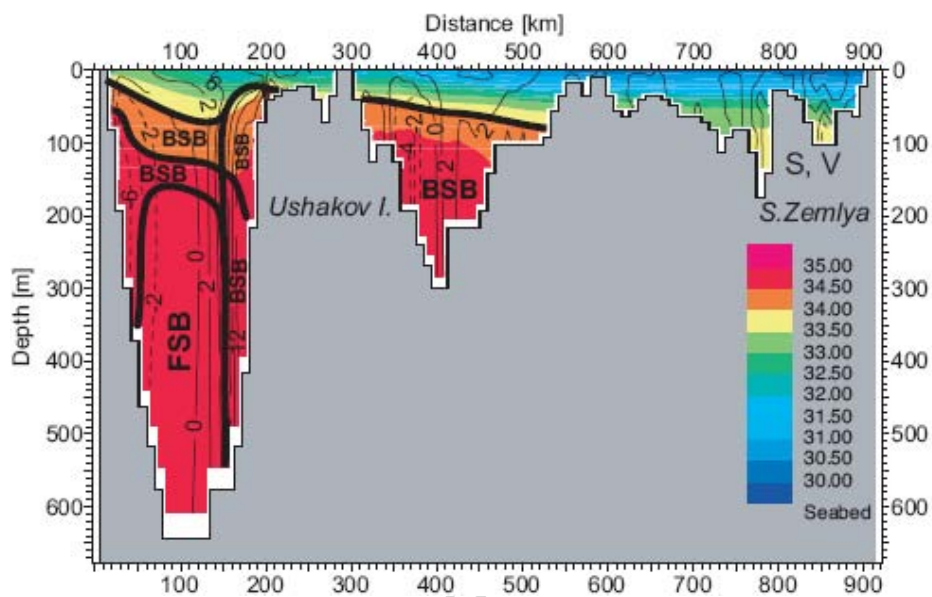


Figure 8b

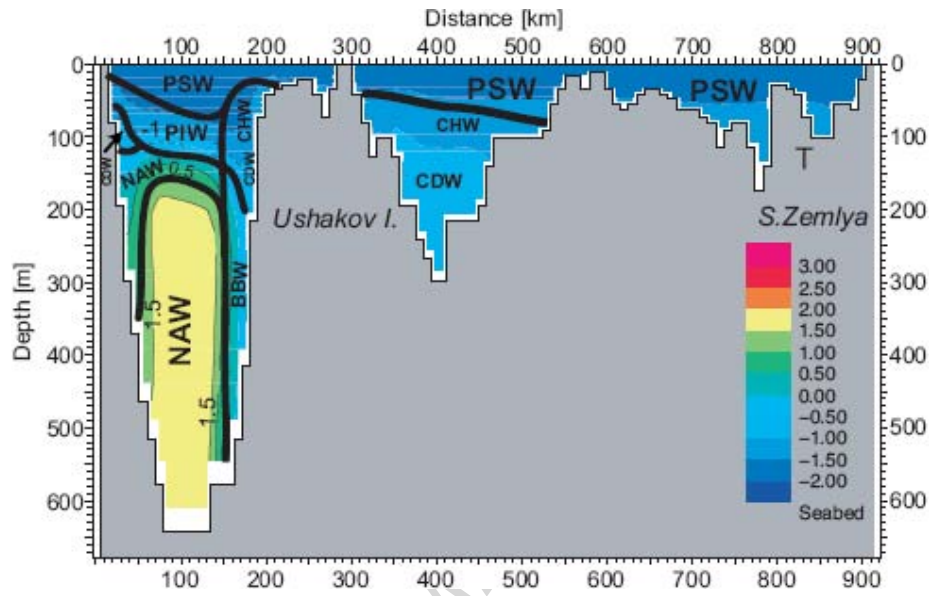


Figure 9a

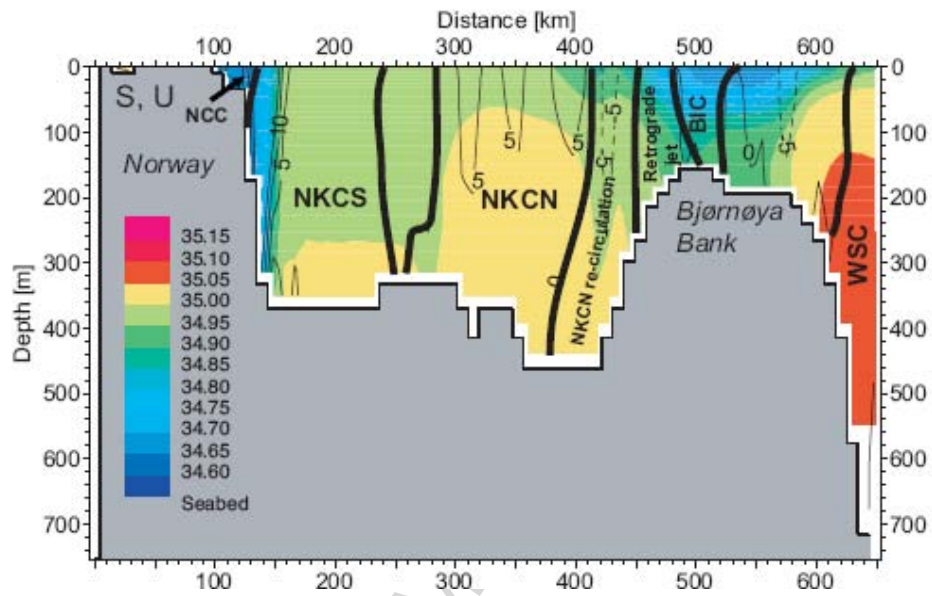


Figure 9b

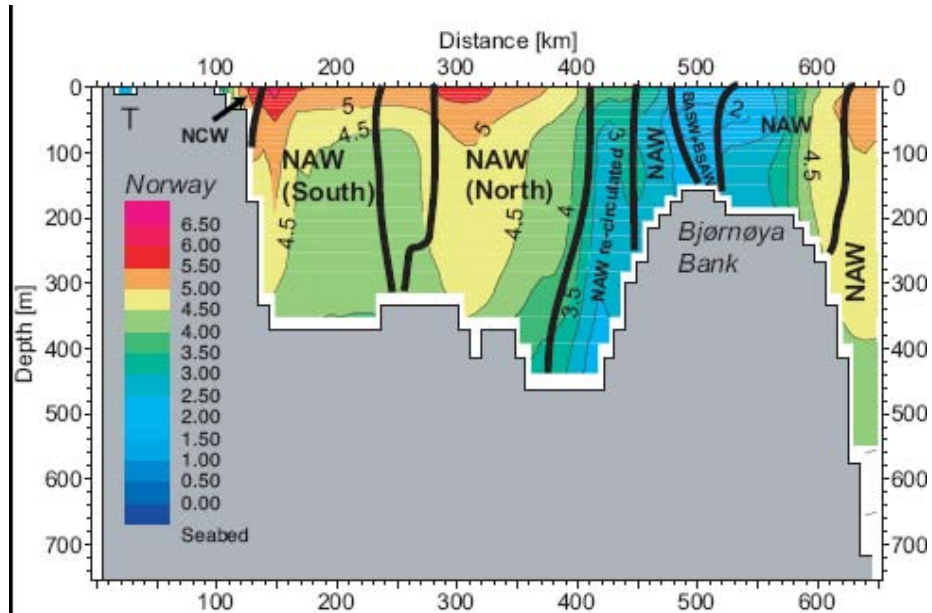


Figure 10

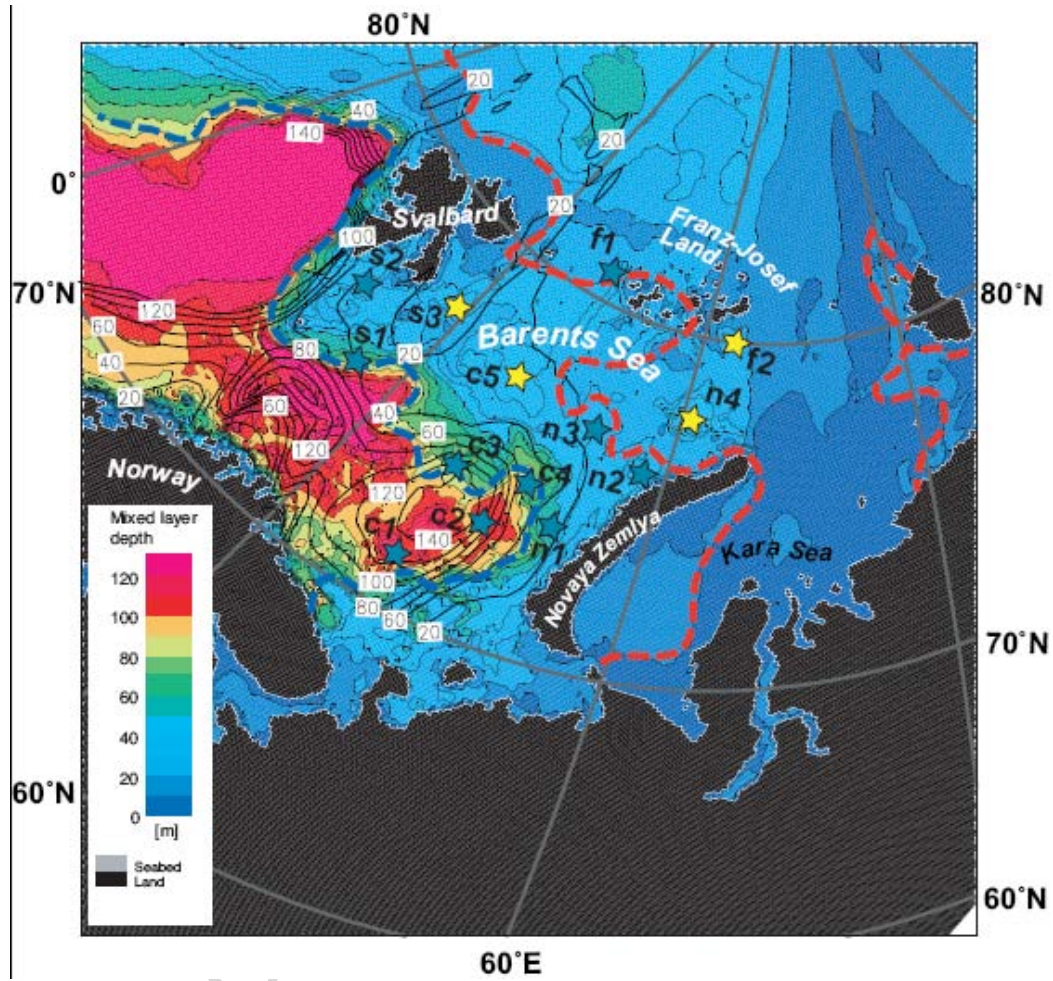


Figure 11a

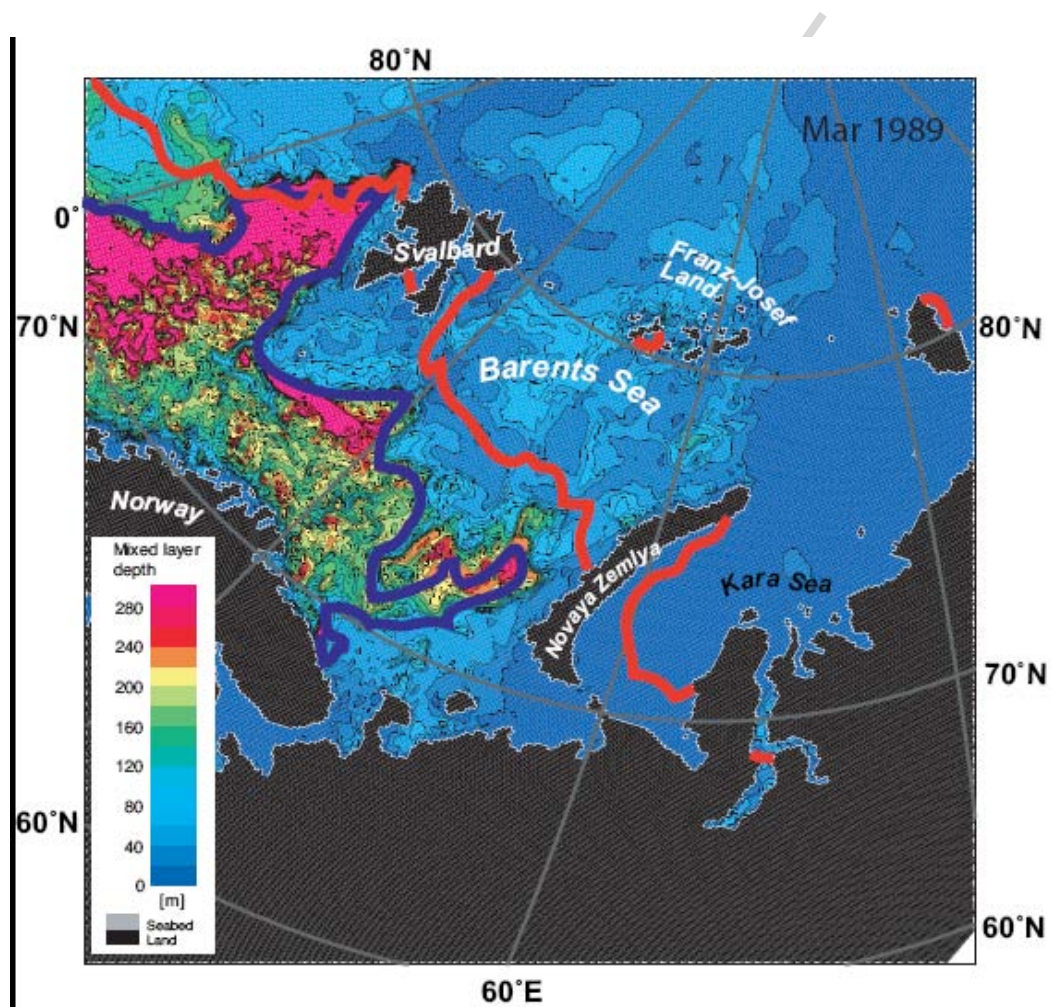


Figure 11b

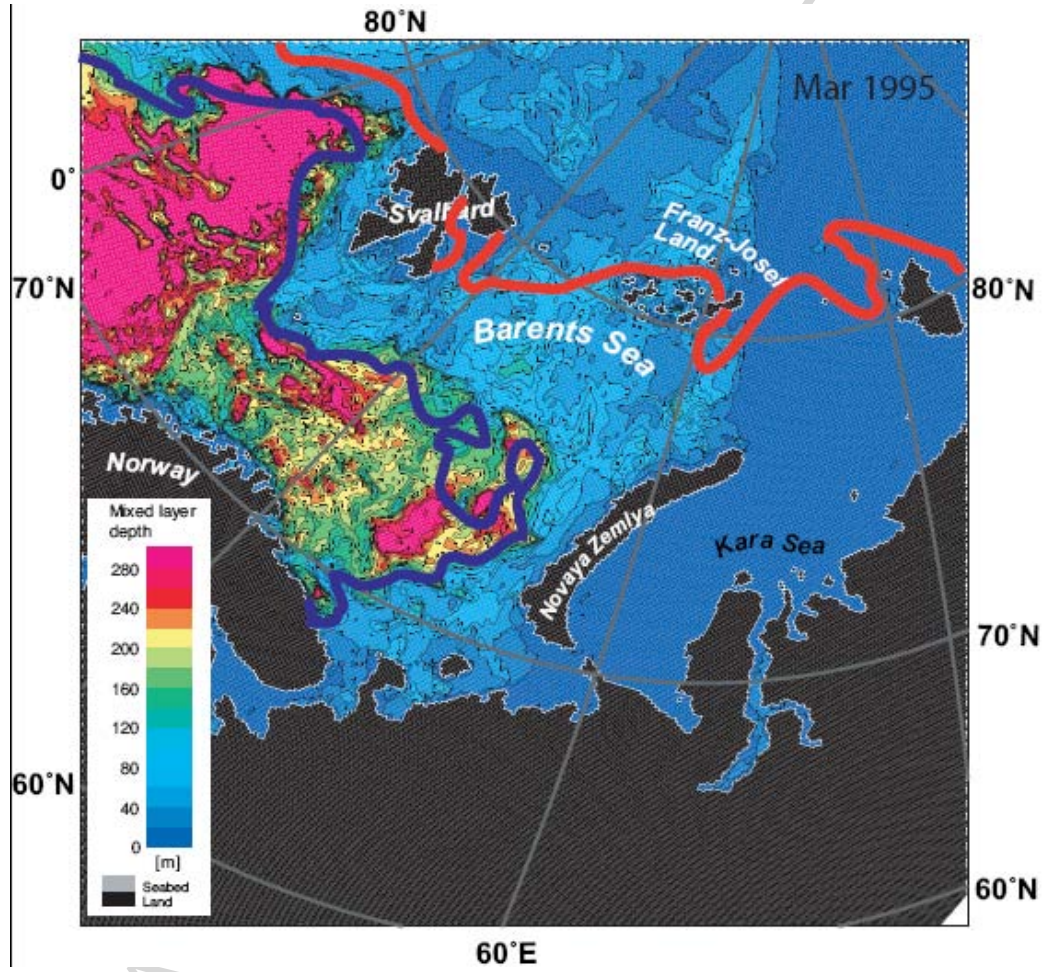


Figure 11c

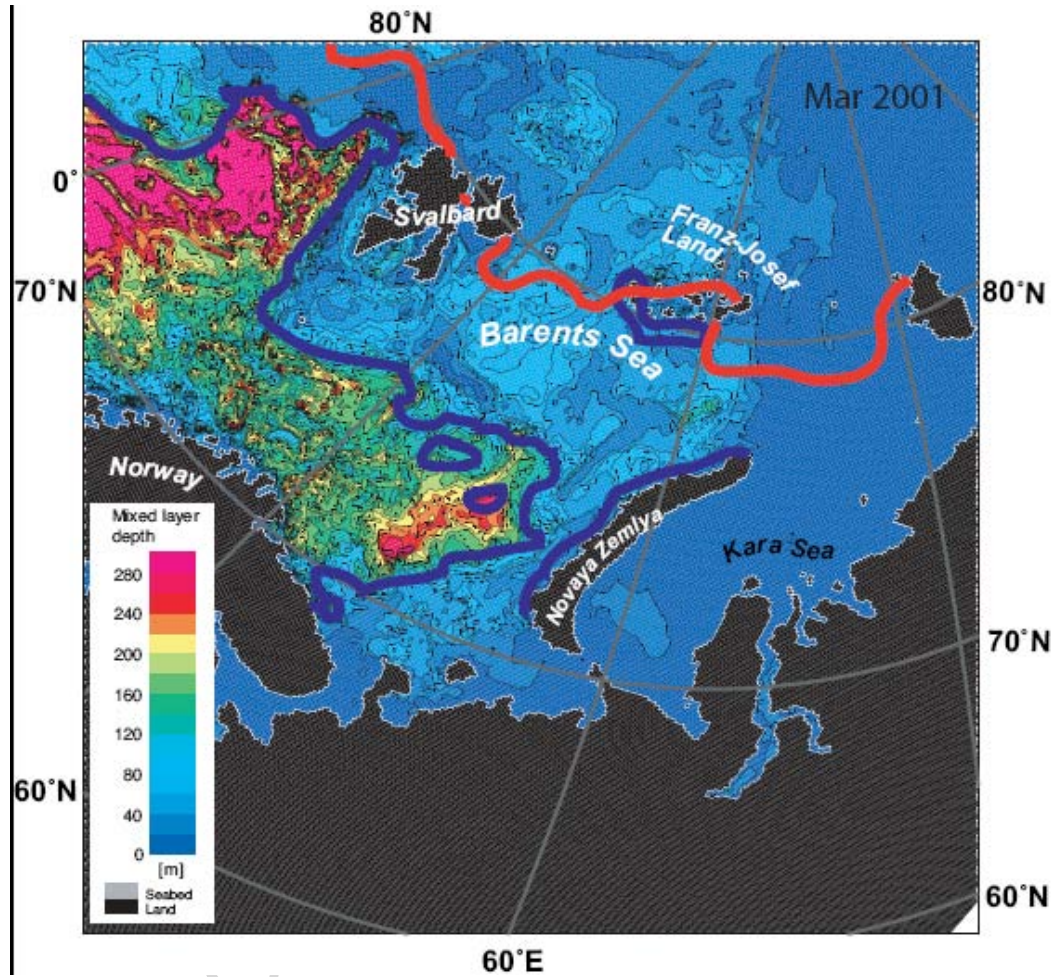


Figure 11d

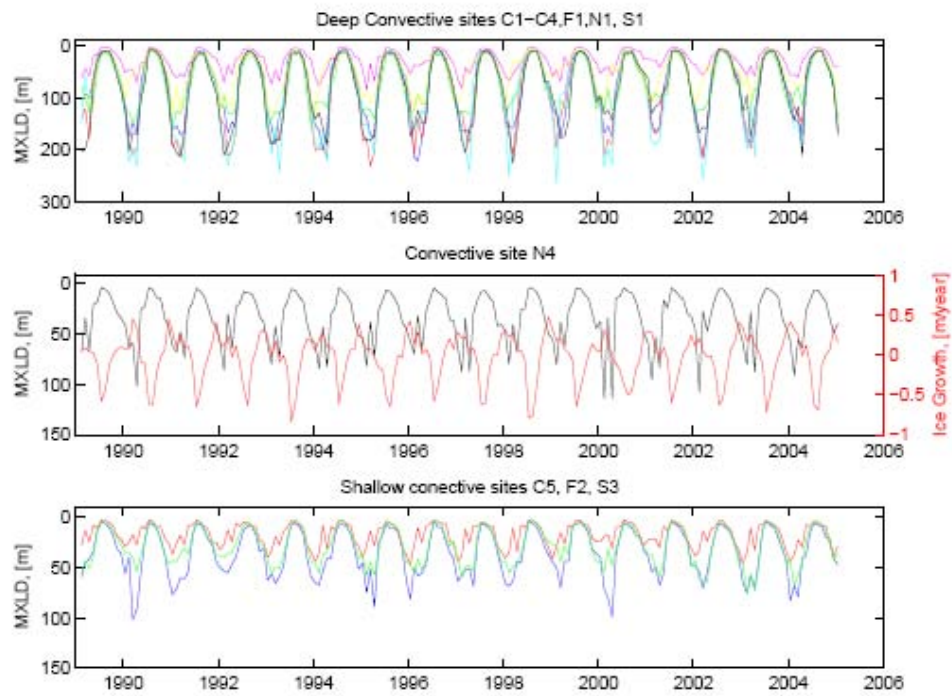


Figure 12

